RAMA: The Research Moored Array for African-Asian-Australian Monsoon Analysis and Prediction

M. J. McPhaden[(1)], G. Meyers[(2)], K. Ando[(3)],Y. Masumoto[(4)], V. S. N. Murty[(5)], M. Ravichandran[(6)], F. Syamsudin[(7)] J. Vialard[(8)], L. Yu[(9)], W. Yu[(10)]

(1) NOAA/Pacific Marine Environmental Laboratory, Seattle, WA, USA (michael.j.mcphaden@noaa.gov), (2) University of Tasmania, Hobart, Australia, (3) Japan Agency for Marine Earth Science and Technology, Yokosuka, Japan, (4) University of Tokyo, Tokyo, Japan, (5) National Institute of Oceanography, Goa, India, (6) Indian National Center for Ocean Information Services, Hyderabad, India, (7) Agency for the Assessment and Application of Technology (BPPT), Indonesia, (8) IRD/Laboratoire d'Océanographie et du Climat: Expérimentation et Approches Numériques Paris, France, (9) Woods Hole Oceanographic Institution, Woods Hole, MA, USA, (10) First Institute of Oceanography, Qingdao, China

Submitted to the *Bulletin of the American Meteorological Society*

27 May 2008

Capsule

A new moored buoy array in the historically data sparse Indian Ocean provides measurements to advance monsoon research and climate forecasting.

Abstract

The Indian Ocean is unique among the three tropical ocean basins in that it is blocked at 25°N by the Asian land mass. Seasonal heating of the land sets the stage for dramatic monsoon wind reversals, strong ocean-atmosphere interactions, and intense seasonal rains over the Indian subcontinent, Southeast Asia, East Africa, and Australia. Recurrence of these monsoon rains is critical to agricultural production that provides life-sustaining support for half the world's population. The Indian Ocean also remotely influences the evolution of El Niño and the Southern Oscillation (ENSO), the North Atlantic Oscillation (NAO), North American weather, and Atlantic hurricane formation. Despite its importance in the regional and global climate system though, the Indian Ocean is the most poorly observed and least well understood of the three tropical oceans.

This article describes the ***R***esearch Moored ***A***rray for African-Asian-Australian ***M***onsoon ***A***nalysis and Prediction (RAMA), a new observational network designed to address outstanding scientific questions related to Indian Ocean variability and the monsoons. RAMA is a multi-nationally supported element of the Indian Ocean Observing System (IndOOS), a combination of complementary satellite and *in situ* measurement platforms for climate research and forecasting. The article describes the scientific rationale, design criteria, and progress towards implementing the array. Initial RAMA data are presented to illustrate how they contribute to improved documentation

and understanding of phenomena in the region. Potential future applications of the data for societal benefit are also described.

1. Introduction

The circulation of the Indian Ocean is unique compared to that of the Pacific and the Atlantic. The Asian landmass blocks the ocean to the north so that currents cannot carry heat from the tropics to higher northern latitudes as in the other oceans. The Indian Ocean also receives heat from the Pacific via the Indonesian Throughflow (Gordon, 2001) while exporting heat to the Atlantic via the Aguhlas Current system (de Ruijter et al, 1999). Ocean-atmosphere interactions in the region is highly dynamic, involving seasonal monsoon wind and current reversals, and significant exchanges of heat across the air-sea interface. Monsoon rains occur each year, supporting agricultural production that provides food for half the world's population. These rains are irregular, however, leading to years of drought or flood that have significant socio-economic consequences (Webster et al, 1998). Failure of Indian summer monsoon rains in 2002 (Waple and Larimore, 2003) and excessive rains in equatorial East Africa in late 2006 (Arguez, 2007) are recent examples of major disasters. Moreover, atmospheric teleconnections carry the effects of Indian Ocean climate anomalies to other regions of the globe, where they affect evolution of El Niño and the Southern Oscillation (ENSO) (McPhaden, 1999; Zhang, 2005), the North Atlantic Oscillation (Hoerling et al, 2001), Atlantic hurricane formation (Maloney and Hartmann, 2000), the atmospheric circulation of the North Pacific (Annamalai et al, 2007) and western U.S. weather (Higgins and Mo, 1997). Thus, the potential benefits derived from improved description, understanding and prediction of the coupled ocean–atmosphere system in the Indian Ocean are enormous. However, the present lack of comprehensive data records for the Indian Ocean severely limits our

knowledge of relevant physical processes and our ability to provide reliable forecasts even one season ahead.

Major observational efforts in the Indian Ocean date back to the International Indian Ocean Expedition of the 1960s (Knauss, 1961; National Research Council, 2000). Since then, many field programs have explored aspects of oceanic and atmospheric circulation, ocean-atmosphere interactions, and ocean biogeochemical cycles related to the monsoons. These programs include the Indian Ocean Experiment (Luyten et al, 1980), the Monsoon Experiment (Krishnamurti, 1985), the World Ocean Circulation Experiment (Siedler et al, 2001), the Tropical Ocean Global Atmosphere program (National Research Council, 1996), the Bay of Bengal Monsoon Experiment (Bhat et al, 2000), the Arabian Sea Monsoon Experiment (Sanjeeva Rao and Sikka, 2005), the Joint Air-Sea Monsoon Experiment (Webster et al, 2002) and the Joint Global Ocean Flux Study (Smith, 2001). However, these programs did not leave a significant legacy of sustained ocean observations in the region (e.g. McPhaden et al, 1998). Development of a tropical Indian Ocean component to the Global Ocean Observing System (GOOS) has progressed very slowly in part because Indian Ocean sea surface temperature (SST) anomalies are most often within the range of observational errors (e.g. Annamalai and Murtugudde, 2004), because there was debate about whether ocean dynamics played a major role in the predictability of those anomalies that were significant, and because "the predictive relationship between Indian Ocean SST and monsoon rainfall have remained especially poorly characterized…" (Clark et al, 2000). Decade-long international programs in the 1980s and 1990s meanwhile focussed heavily on phenomena such as ENSO in the Pacific and tropical Atlantic climate variability where ocean-atmosphere

interactions were better understood and model prediction efforts were more advanced. The remoteness of the Indian Ocean from first world countries of North America, Europe, and Asia was also a factor in the relatively slow development of Indian Ocean GOOS.

The past 10 years though has seen a rebirth of interest in the Indian Ocean stimulated by the prominence of the 1997 Indian Ocean Dipole Zonal Mode (IODZM) event (Saji et al, 1999; Webster et al, 1999; Murtugudde et al, 2000). This event highlighted the dramatic nature and climatic consequences of ocean atmosphere interactions originating in the Indian Ocean. The event also drew attention to the relative dearth of measurements in the Indian Ocean and the opportunities to develop a systematic and sustained ocean observing system there.

This paper describes the rationale for, and initial implementation of, a sustained, basin-scale moored buoy array referred to as the ***R***esearch Moored ***A***rray for African-Asian-Australian ***M***onsoon ***A***nalysis and Prediction (RAMA[1]). The array complements other elements of the recently designed Indian Ocean Observing System (IndOOS) which collectively represents an Indian Ocean contribution to GOOS (CLIVAR-GOOS Indian Ocean Panel, 2006; Meyers and Boscolo, 2006). IndOOS in general, and RAMA in particular, address the need to develop a comprehensive data base of high quality long term measurements in the Indian Ocean suitable for climate research and forecasting. The broad range of time scales and rapid changes that can occur in the Indian Ocean dictate the need for a moored buoy array providing time series data with high temporal resolution as an essential element of IndOOS. In this respect, RAMA is the Indian Ocean

[1] In Hindu mythology, Rama is an ancient king of India and the hero of the epic "Ramayana".

94 equivalent of the Tropical Atmosphere Ocean/Triangle Trans Ocean Buoy Network
95 (TAO/TRITON; McPhaden et al, 1998; Kuroda and Amitani, 2000) and the Prediction
96 and Research Moored Array in the Tropical Atlantic (PIRATA; Bourles et al, 2008),
97 which respectively anchor basin scale observing systems in the tropical Pacific and
98 Atlantic Oceans. Though RAMA is targeted at understanding and prediction of the east
99 African, Asian, and Australian monsoons, it will benefit nations outside the Indian Ocean
100 region because of atmospheric teleconnections that influence the far field. In addition,
101 RAMA is based on the same technology used in TAO/TRITON and PIRATA and so
102 provides data in real-time that will contribute to improved weather and marine forecasts,
103 particularly those related to tropical cyclones and storm surge. Indeed, real-time data
104 from RAMA buoys have already been used cyclone forecasting, as in the case of cyclone
105 Nargis which developed in the Bay of Bengal in late April and early May 2008.[2]
106 The remainder of this paper is organized as follows. We first briefly review the
107 range of phenomena that motivate the need for understanding and predicting climate
108 variability in the Indian Ocean region. Emphasis is on the fast time scales and the upper
109 ocean north of 30°S where RAMA will have their greatest impact. The reader is referred
110 to Schott et al (2008) for a more complete account of Indian Ocean phenomenology
111 including western boundary currents , the Indonesian Throughflow, major surface
112 currents, and the cross-equatorial overturning circulation. We then describe IndOOS and
113 the design criteria for RAMA, followed by a progress report on RAMA implementation.

[2] Nargis was the worst natural disaster to affect the region since the Asian tsunami in December 2004. It made landfall in Myanmar, leaving in its wake a swath of destruction that included over 130,000 dead and missing and billions of dollars in economic losses.

Examples of RAMA data are presented to illustrate their value for research applications, after which we conclude with a brief summary and discussion.

2. Indian Ocean Phenomenology

Hallmark attributes of the Indian Ocean climate system are the dramatic reversals of the surface winds propelled by seasonally varying land-ocean temperature contrasts, and the seasonally varying wind-driven ocean currents that modulate the evolution of SST (Fig. 1; see also Schott and McCreary, 2001). Associated with monsoon wind variations are pronounced seasonal shifts in atmospheric convection and rainfall over East Africa, southern and eastern Asia, and northern Australia. Collectively, these variations are a regional manifestation of seasonal changes in the Hadley and Walker Circulations, which extend throughout the global tropics.

In boreal winter, Northeast Monsoon winds converge with Southeast trade winds in the Intertropical Convergence Zone (ITCZ) located between 5°-12°S. These wind systems drive a surface ocean circulation that features broad, westward flowing currents on either side of the equator—the Northeast Monsoon Current and South Equatorial Current—and a southward flowing Somali Current along the east coast of Africa. Sandwiched between the two westward currents is the eastward flowing Equatorial Countercurrent, in geostrophic balance with meridional density contrasts in the Seychelles-Chagos thermocline ridge region (Hermes and Reason, 2008; Yokoi et al, 2008). This thermocline ridge, formed by wind stress curl driven upwelling in the ITCZ, is very shallow. Its proximity to the surface creates a zone of intense ocean-atmosphere interaction on multiple time scales which can, for example, remotely influence subsequent development of summer monsoon rainfall along the western Ghats (Vecchi

and Harrison, 2004; Izumo et al, 2008) and the circulation over the North Pacific (Annamalai et al, 2005).

Wind and circulation patterns in boreal summer are radically different from those in boreal winter. Southwest Monsoon winds cause a reversal of the westward flowing currents north of the equator and weakening of the countercurrent and thermocline ridge. Intense wind-driven coastal upwelling during summer off the Horn of Africa leads to cooling and, through the supply of nutrient rich thermocline water, high biological productivity in the Arabian Sea. This upwelling is fed by a cross equatorial circulation cell that is unique to the Indian Ocean, with source waters formed in the southeastern Indian Ocean (~20°-30°S) flowing northward at thermocline depth to the Arabian Sea (Schott et al, 2004). SSTs in Bay of Bengal on the other hand remain relatively high during summer, stoking the growth of cyclones that often have devastating impacts on surrounding countries. High Bay of Bengal SSTs result from strongly salt stratified mixed layers, supplied by fresh water from river runoff and open ocean rainfall, which inhibit mixing with cold subsurface thermocline waters (Shenoi et al, 2002).

During the transition seasons between the Northeast and Southwest Monsoons, winds along the equator are westerly. These winds force the eastward flowing "Wyrtki Jets" (Wyrtki, 1973) in April-May and October-November of each year. The Wyrtki Jets are important in transporting mass from west to east along the equator and play an important role in the seasonal heat balance of the basin. They are also dynamically linked to variability off of Sumatra and Java through equatorial and coastal waveguide processes (Wijffels and Meyers, 2004).

159 Embedded within the seasonally varying monsoons are energetic intraseasonal
160 oscillations (or ISOs) on shorter weekly to monthly time scales. The best known form of
161 ISO is the Madden-Julian Oscillation (MJO), an eastward propagating wave-like
162 phenomenon in the atmosphere with periods of roughly 30-60 days (Madden and Julian,
163 1994; Zhang, 2005; Fig. 2). The MJO is spawned over the Indian Ocean through
164 convectively coupled dynamic instabilities and subsequently propagates eastward around
165 the globe at upper tropospheric levels as a planetary scale fluctuation in the wind field.
166 Variability in surface winds and deep convection are most energetic in regions of warm
167 SST ($\geq 27°C$), where interaction with the oceanic mixed layer plays an important role in
168 organizing the MJO (Waliser et al, 1999). Ocean-atmosphere interactions on
169 intraseasonal time scales are particularly strong during boreal winter in the vicinity of the
170 shallow Seychelles-Chagos thermocline ridge where SST is sensitive to surface wind,
171 cloudiness, and thermocline depth variations (Duvel and Vialard, 2007). Along the
172 equator, intraseasonal wind forcing generates energetic eastward propagating oceanic
173 Kelvin waves (Han, 2005; Fu, 2007) which, upon encountering Sumatra, continue
174 poleward as coastally trapped waves. The majority of coastally trapped intraseasonal
175 wave energy propagating southeastward off of Sumatra and Java eventually leaks into the
176 Indonesian Seas through the Lombok Strait where it affects Throughflow transports
177 (Syamsudin et al, 2004).
178 The MJO is strongest in boreal winter and spring in the southern tropics, with a
179 secondary peak during boreal summer north of the equator (Zhang, 2005). In the
180 summertime, the MJO spins off cloud and rain bands near the equator that propagate
181 poleward over the Bay of Bengal, leading to alternating "active" periods of enhanced

182 rainfall and “break” periods of reduced rainfall (Madden and Julian, 1994). The number
183 and duration of active/break periods in a particular year determines the net seasonal
184 monsoon rainfall. For this reason intraseasonal oscillations are often referred to as the
185 “building block of the monsoons.”

186 There are significant multi-time scale interactions involving the MJO that
187 complicate its dynamics and impacts. For instance, the MJO strongly modulates
188 variability associated with the Wyrtki Jets (Han et al, 2004; Masumoto et al, 2005;
189 Sengupta et al, 2007). The diurnal cycle is important in modulating MJO SST variability
190 and ocean feedbacks to the atmosphere (Woolnough et al, 2007). Synoptic time scale
191 cyclones often develop in association with the MJO in both the Indian and Pacific Oceans
192 (Liebmann et al, 2004; Bessafi and Wheeler, 2006; Seiki and Takayabu, 2007). Positive
193 IODZM events (see below) tend to suppress the MJO and as well as higher frequency
194 atmosphere fluctuations as a result of the reduced convection over the eastern Indian
195 Ocean (Shinoda and Han, 2005). Farther afield, propagation of the MJO into the western
196 Pacific, especially in boreal winter and spring, affects the evolution of ENSO
197 (McPhaden, 1999; Zhang, 2005). The MJO likewise influences the development of
198 Atlantic hurricanes via modulation of planetary scale upper level divergence fields
199 (Maloney and Hartmann, 2000) and winter storms along the west coast of the U.S.
200 (Higgins and Mo, 1997).

201 There are other notable intraseasonal variations in the Indian Ocean and
202 atmosphere besides the MJO. For example, 10-20 day period fluctuations in meridional
203 winds near the equator excite prominent biweekly period mixed Rossby-gravity waves in
204 the ocean (Sengupta et al, 2004). There is also a spectral peak in sea level variability at

205 periods near 90 days that Han (2005) attributes to a wind-forced basin scale oceanic
206 resonance.

207 The Indian Ocean is characterized by considerable interannual variability, the
208 most prominent mode of which is the response to remote forcing from ENSO (Yamagata
209 et al, 2004; Schott et al, 2008). An eastward shift in the ascending branch of Walker
210 circulation into the central Pacific during El Niño leads to anomalous subsidence,
211 suppressed convection, high atmospheric surface pressure, and anomalous easterlies over
212 the Indian Ocean. El Niño's impact on precipitation includes reduced Indian summer
213 monsoon rainfall, reduced rainfall in South Africa and Indonesia, and enhanced rainfall in
214 equatorial east Africa. In boreal spring following the peak of El Niño, basin scale
215 warming occurs due to a combination increased surface heat fluxes and, south of the
216 equator, to a downwelling Rossby wave forced by anomalous ENSO-induced surface
217 wind stresses (Xie et al, 2002; Yu et al, 2005; Schott et al, 2008). The amplitude of this
218 warming is relatively small compared to that in the tropical Pacific, but it persists into the
219 following boreal summer, increasing rainfall over much of the basin (Yang et al, 2007).
220 Also, in the southwestern tropical Indian Ocean, elevated SSTs linked to downwelling
221 Rossby wave dynamics lead to increased tropical cyclone activity (Xie et al, 2002).
222 Oceanic and atmospheric anomalies of opposite sign are evident in the Indian Ocean
223 region associated with La Niña events.

224 Another prominent mode of interannual variability in the Indian Ocean is the
225 IODZM, positive events of which are characterized by anomalously cold SSTs and
226 suppressed atmospheric convection off Java and Sumatra, warm SSTs and enhanced
227 convection off east Africa, easterly wind anomalies along the equator, and a weak boreal

fall season Wyrtki Jet (Fig. 3). The IODZM is a mode of coupled ocean-atmosphere variability that, like ENSO, develops via feedbacks between zonal wind stress, SST and thermocline depth anomalies. Unlike ENSO though, it is shorter lived and confined mostly to the boreal fall season. Annual mean winds along the equator are westerly in Indian Ocean, tilting the thermocline down to the east. Thus, it is only during the normal September to November upwelling season off the coast of Java and Sumatra when the thermocline is brought close enough to the surface that ocean-atmosphere feedbacks can take hold. After that, the strong seasonality associated with the onset of the Northeast Monsoon overwhelms any SST anomalies in this upwelling region that may have developed during the previous summer and fall.

The most recent positive IODZM events of significant amplitude occurred in 1994, 1997, and 2006 (Fig. 3e). These events typically lead to above normal rainfall in East Africa, India, and Southeast Asia and dry conditions in Indonesia and Australia (Yamagata et al, 2004). Far field impacts of the IODZM have also been reported on the seasonal climate of East Asia (i.e., China, Japan and Korea), Brazil, and Europe (*op. cit.*). Negative IODZM events develop with anomalies and climatic impacts roughly opposite to those of positive events.

There is a tendency for positive IODZM events to co-occur with El Niño and negative events with La Niña (Meyers et al, 2007). These co-occurrences have complicated the identification of IODZM vis-à-vis ENSO climate impacts and have raised the question of whether the IODZM is fundamentally tied to ENSO (e.g., Chang et al, 2006). However, co-occurrences with ENSO do not account for all IODZM events and the dynamical ocean response to ENSO vs. purely IODZM wind forcing is not identical

(Yu et al, 2005). Thus, while ENSO may be an important triggering mechanism, the IODZM appears to exist as an independent mode of climate variability (Schott et al, 2008).

In addition to interannual variability, the Indian Ocean also experiences longer term decadal variations and trends. For example, there is a decadal modulation in the frequency of IODZM events (Ashok et al, 2004), in the relationship between ENSO and the IODZM (Schott et al, 2008), and in the relationship between ENSO and Indian summer monsoon rainfall (Krishna-Kumar et al, 1999). Decadal changes in Indian Ocean circulation have been documented, including a decrease in strength of the Indonesian Throughflow since 1976 (Wainwright et al., 2008) and an intensification around 2000 of the subtropical cell (Lee and McPhaden, 2008), which links upwelling in the Seychelles-Chagos thermocline ridge to source waters formed between 20°-30°S in the southeastern basin. Superimposed on these decadal variations are significant multi-decadal warming trends in SST (Cane et al, 1997) and increases in upper ocean heat content (Levitus et al, 2005) that may plausibly be attributed to anthropogenic greenhouse gas forcing. The SST trend has been linked to drought in the African Sahel (Giannini et al., 2003) and the northern hemisphere mid-latitudes (Hoerling and Kumar, 2003). Latent heat fluxes have increased steadily since the early 1980s over the Indian Ocean (Yu and Weller, 2007) suggesting that changes in surface fluxes are a response to, rather than the cause of, this SST trend. It is likely that ocean dynamics plays a role in producing the observed SST trend, although the precise mechanisms remain uncertain (Alory et al, 2007).

In summary, there is a broad spectrum of phenomena in the Indian Ocean, ranging from diurnal to decadal time scales, that contributes to the observed variability. Quantitative understanding of these phenomena, and how they interact with one another, is undermined though by a sparsity of data. Unlike in the Pacific Ocean where systematic observations as part of the ENSO observing system were initiated in the early 1980s, there are no high quality multi-decade in situ data records in the upper Indian Ocean except for those from a few ship-of-opportunity expendable bathythermograph (XBT) lines (Feng et al, 2001; Feng and Meyers, 2003). These limitations make it difficult to assess with confidence whether the Indian Ocean-atmosphere system is changing, or may change, as a result of greenhouse gas forcing (Harrison and Carson, 2007).

Data limitations also constrain our ability to develop, initialize, and validate coupled ocean-atmosphere forecast models for monsoon prediction. Experimental forecasting with these models is in its infancy, and there are preliminary indications that skillful seasonal forecasts in the Indian Ocean region may be possible at 2-3 season lead times based on ENSO and IODZM influences (Luo et al, 2007; Cherchi et al, 2007). Present levels of skill are limited by poor initialization of the subsurface ocean (Wajsowicz, 2005), systematic errors in ocean and atmospheric models, and the general inability of either atmospheric general circulation models or coupled ocean-atmosphere models to accurately simulate intraseasonal variability like the MJO (Slingo et al, 1996; Zhang, 2005). Intraseasonal oscillations are a major influence on the evolution of the monsoons and ENSO and there is evidence to suggest that elements of this intraseasonal variability may be predictable up to 30 days in advance (Webster and Hoyos, 2004;

295 Miura et al, 2008). Thus, the fact that ISOs are not well represented in dynamical
296 prediction models represents a major challenge in climate and weather forecasting.

297 3. RAMA as a contribution to IndOOS

298 3.1 IndOOS

299 The International GOOS program and the Climate Variability and Predictability
300 (CLIVAR) component of the World Climate Research Program (WRCP) established an
301 Indian Ocean Panel (IOP) in 2004 to design, and guide the implementation of, a basin-
302 scale, integrated Indian Ocean observing system for climate research and forecasting. The
303 IOP focused on developing a strategy for *in situ* measurements to complement existing
304 and planned satellite missions for surface winds, sea level, SST, rainfall, salinity, and
305 ocean color. The resulting system, referred to as IndOOS (Fig. 4), is based on proven
306 technologies, including moorings, Argo floats, ship-of-opportunity measurements,
307 surface drifters, and coastal tide gauge stations (CLIVAR-GOOS Indian Ocean Panel,
308 2006; Meyers and Boscolo, 2006). Current efforts to observe the Indonesian
309 Throughflow and eastern and western boundary currents were also incorporated into the
310 design. Transmission of data to shore in real-time via satellite relay, where feasible, was
311 given high priority to promote use of the data in climate analysis and forecast products.
312 Network design emphasized the measurement of physical climate variables but
313 recognized that as the science matures and technology advances, widespread inclusion of
314 biogeochemical measurements to support studies of the ocean carbon cycle and
315 ecosystems dynamics would also be possible.

316 3.2 RAMA

A key element of IndOOS is the basin-scale moored buoy array which we call RAMA (Fig. 5). Some of the Indian Ocean programs described in the Introduction collected 1-3 year long time series records either near the equator (Knox, 1976; Reppin et al, 1997) or in the Arabian Sea (Rudnick et al, 1997). Despite these noteworthy efforts though, there has been no plan until now for a coordinated, multi-national, basin-scale sustained mooring array like TAO/TRITON in the Pacific and PIRATA in the Atlantic.

RAMA addresses the need for such a plan. It is intended to be marginally coherent in latitude and longitude for defining large-scale patterns of variability on intraseasonal and longer time scales. Data include high temporal resolution measurements (hourly and daily averages in real-time, 1- to 10-minute samples internally recorded) of surface meteorological variables, SST, and upper-ocean temperature, salinity and velocity. These time series measurements at fixed locations are especially well suited for studying mixed-layer dynamics, ocean-atmosphere interactions, and multi-time scale variability related to the MJO and other intraseasonal phenomena.

The planned array consists mainly of 38 Autonomous Temperature Line Acquisition System (ATLAS) and Triangle Trans Ocean Buoy Network (TRITON) surface moorings (see box). Four subsurface Acoustic Doppler Current Profiler (ADCP) moorings are located along the equator where geostrophy breaks down and direct current measurements are necessary. A fifth ADCP mooring is also located in the upwelling zone off the coast of Java where the SST anomalies associated with the IODZM first develop. This mooring is near the northern terminus of the frequently repeated Australia-to-Indonesia XBT line (Fig. 4) providing upper ocean temperature observations at weekly intervals. The primary focus of the array is the upper 500 m, where the ocean and

340 atmosphere most immediately communicate with one another and where intraseasonal-to-
341 decadal time scale variability is most pronounced. However, in addition to the 38 surface
342 and 5 ADCP moorings, three subsurface moorings along the equator at 77°E, 83°E, and
343 93°E are designed to monitor ocean currents down to 4000 m (Murty et al, 2006).

344 The array is intended to cover the major centers of ocean–atmosphere interaction
345 in the open ocean away from western boundary current regions and the Indonesian
346 marginal seas. These regions include the Arabian Sea and the Bay of Bengal; the
347 equatorial waveguide where wind-forced intraseasonal and semi-annual current variation
348 is prominent; the eastern and western poles of the IODZM; the thermocline ridge
349 between 5-12°S, where wind-induced upwelling and Rossby waves affect SST; the
350 southwestern tropical Indian Ocean, where ocean dynamics and air–sea interaction affect
351 cyclone formation (Xie et al., 2002); and the southeastern basin where source waters of
352 the cross equatorial and subtropical circulation cells are formed (Schott et al, 2004).
353 Numerical model design studies have assessed the adequacy of the array to achieve its
354 purposes in the context of other observing system components. Alternative sampling
355 strategies have also been evaluated with the conclusion that the proposed array
356 configuration is scientifically sound and cost-effective (Vecchi and Harrison, 2007; Oke
357 and Schiller, 2007).

358 Surface heat and moisture fluxes are important in determining mixed layer
359 temperature and salinity variability. However, surface heat and moisture flux
360 climatologies are poorly known in the Indian Ocean (Yu and McCreary, 2004;
361 Yaremchuk, 2006; Yu et al, 2007) and in several regions annual means in net surface heat
362 flux from presently available climatologies typically differ by 30-40 W m^{-2} (Fig. 6).

Hence, in each of the key regions described above, plans call for at least one specially instrumented surface mooring as a surface flux reference site.

ATLAS and TRITON mooring data are telemetered to shore in real-time from the via the Service Argos satellite relay system. Service Argos then places these data on the Global Telecommunications System for transmission to operational weather, climate, and ocean forecasting centers. Internally recorded data from all moorings are post-processed and quality controlled on recovery, after which they are then posted on World Wide Web for public distribution (see box on RAMA Moorings). The RAMA data policy is based on the principle of free, open, and timely access to all data from the array.

4. Progress Towards Implementation of RAMA

At present, RAMA is 39% complete, with 18 of the 46 total mooring sites occupied (Figure 5). Nations that that have provided mooring equipment, ship time, personnel, and/or logistic support so far include Japan, India, the United States, Indonesia, China, and France. Contributing organizations and their year of initial involvement are described in the Implementation Time Line side box. Formal bilateral agreements are either under development or approved between agencies in the various partner countries to help complete and sustain the array. The CLIVAR-GOOS Indian Ocean Panel and the CLIVAR Tropical Moored Buoy Implementation Panel provide scientific and technical guidance, respectively, for implementation of RAMA.

The array will require a reliable, regular supply of ship time to fully implement since the surface moorings have a design lifetime of one year and must be replaced annually. Making reasonable assumptions about ship speeds, carrying capacity, and ports of call around the Indian Ocean, McPhaden et al (2006) estimated that a minimum

386 approximately 140 days of dedicated ship time per year will be required to maintain the
387 array once complete. For perspective, this requirement is about half that needed to
388 maintain the 70 mooring TAO/TRITON array in the Pacific and about twice that needed
389 to maintain the smaller 18 mooring PIRATA array in the Atlantic.

390 The greatest impediment to implementation, assuming adequate financial
391 resources and ship time can be found, is vandalism by fishing vessels. Surface buoys are
392 effectively Fish Aggregation Devices (FADs) that attract fish and, consequently,
393 fishermen. Vandalism occurs primarily in pursuit of tuna and affects TAO/TRITON and
394 PIRATA as well as RAMA. Strategies to mitigate vandalism include engineering design
395 improvements to the moorings and outreach to the fishing community. Data losses can
396 also be minimized by scheduling cruises to repair or replace moorings at yearly or more
397 frequent intervals.

398 5. Data and Research Applications

399 RAMA, even though in the initial stages of development, is providing valuable
400 data for describing and understanding variability in the Indian Ocean. For example, a
401 pronounced semi-annual cycle in upper ocean temperature, salinity and zonal velocity is
402 evident in the first 3-years of data from near equatorial moorings at 90°E (Fig. 7). Hase et
403 al (2008) relate this variability to remote zonal wind forcing in the central Indian Ocean
404 associated with the monsoon transitions. Upward phase propagation at semi-annual
405 periods in both temperature and zonal velocity is presumably the signature of wind forced
406 equatorial Kelvin waves. This vertical propagation is consistent with, but more sharply
407 defined than, that evident in equatorial time series collected during INDEX in the 1970s
408 (McPhaden, 1982; Luyten and Roemmich, 1982). The subsurface salinity maximum

centered near 100-150 m at 90°E (Fig. 7b) is due to eastward transport along the equator of high salinity water originating in the southern hemisphere subtropics and the Arabian Sea (Taft and Knauss, 1967; Schott et al, 2004). Semi-annual increases in maximum salinity values in this subsurface layer are most likely the response to increases in eastward velocity associated with the semi-annual Wyrtki Jets.

Superimposed on these semi-annual variations are energetic 30-50 day period oscillations, which presumably reflect the effects of wind (e.g., Fig. 8a), heat flux, and fresh water forcing on intraseasonal scales. Intraseasonal oscillations are largest for temperature in the thermocline (Fig. 7a) and largest for salinity and zonal velocity in the surface mixed layer (Figs. 7b and 8b). Meridional velocity is most strongly influenced on intraseasonal time scales by 10-20 day period oscillations (Fig. 8c) which are evident not only in the upper 400 m but also at depths greater than 2000 m from the deep ocean moorings along the equator. Sengupta et al. (2004) identified these oscillations as wind forced mixed Rossby-gravity waves.

Interannual variability associated with the 2006 IODZM event was captured by the moored array as illustrated in the time series from 0°, 80.5°E for two contrasting periods: October-November 2004 and October-November 2006 (Fig. 9). Compared to late 2004, which was near normal in terms of IODZM activity (Fig. 3e), zonal surface winds and the zonal mixed layer currents they forced along the equator largely flowed in the opposite direction, i.e. to the east, in late 2006 (Fig. 9a, b). The eastward currents drained the eastern basin of upper ocean mass, which lead to shoaling of the thermocline at 0°, 80.5°E (Fig. 9c). Also, while SST was only slightly warmer than usual at 0°, 80.5°E as would be expected for a mooring located outside the IODZM SST index

regions, mixed layer salinity shows a dramatic drop of over 1 psu in late 2006 relative to late 2004, consistent with enhanced convection in the central basin (Fig. 3c) and equatorward flow of low salinity water from the Andaman Sea (Murty et al, 2008). The in situ observations thus add information on details of upper ocean variability that cannot be measured by satellites. At the same time, the in situ provide data can be used to validate satellite-based products for surface winds, SST, mixed layer currents, and rainfall. It is also interesting to note that the meridional component of mixed layer velocity in Fig. 9b exhibits very regular biweekly oscillations as observed in the 0°, 90°E ADCP data (Fig. 8c) and in the deep ocean moorings along the equator (Sengupta et al, 2004).

Data from the mooring at 8°S, 67°E in the region of the Seychelles-Chagos thermocline ridge illustrate ocean-atmosphere interactions associated with the passage of tropical cyclone Dora (Fig. 10). Dora began as a tropical disturbance northeast of the buoy in the vicinity of Diego Garcia (7°S, 72°E) in late January 2007. As this disturbance migrated in south-southwesterly direction, it intensified to named tropical storm strength on January 30 and to tropical cyclone strength on February 1. Dora reached peak intensity of over 100 kts (51 m s^{-1}) on February 3 when it was centered near 18°S, 67°E. Afterwards, it continued to track to the southwest, eventually dissipating by February 12.

Dora passed near the buoy in the early stages of its development (January 25-29) before it became a named tropical storm. Its effects in the real-time daily averaged data can be seen in the sudden change in wind speed and direction, increase in precipitation, decrease in atmospheric pressure, and decrease in incoming shortwave radiation at the buoy site in late January 2007 (Fig. 10, left panel). Also evident in late January are

455 abrupt cooling and freshening of the surface mixed layer associated with decreased
456 surface heat fluxes and increased fresh water fluxes. Internally recorded 1- to 10-minute
457 data recovered from the buoy show even greater detail during the last week of January
458 2007 (Fig. 10, right panel). One sees for example a very sharp drop in surface salinity and
459 temperature associated with a nighttime rain event on January 24. Also, SST dropped in a
460 very stepwise fashion by 2°C in week. Periods of very low insolation on rainy (and
461 presumably cloudy) days are evident. There is also a pronounced solar semi-diurnal tide
462 in atmospheric surface pressure. These data are being analyzed to quantitatively address
463 the relative roles of surface fluxes, vertical turbulent mixing, and horizontal advection in
464 the heat and salt balances for this particular period (Foltz and McPhaden, 2008).

465 RAMA mooring data can also be used to identify deficiencies in currently
466 available surface flux products as a stimulus to their possible improvement. For example,
467 surface heat fluxes were calculated from data at three of RAMA mooring sites for
468 comparison with numerical weather prediction (NWP) model flux products, the
469 International Satellite Cloud Climatology Project (ISCCP) radiation product (Zhang et al,
470 2004) and an objectively analyzed (OA) turbulent heat flux product (OA-Flux; Yu and
471 Weller, 2007). Results (Fig. 11) indicate that that ISCCP overestimates solar radiation
472 and underestimates longwave radiation at these sites. The NWP products significantly
473 overestimate latent heat fluxes such that the net heat flux into the ocean is underestimated
474 by 40-60 W m^{-2} at 0°, 80.5°E. This heat flux deficit, if accumulated in a 50 m thick mixed
475 layer over three months, would translate into a temperature error of ~2°C, which is
476 equivalent to the seasonal range of SST at this location. The OA-Flux product slightly

underestimates latent heat fluxes at all three locations, but is a significant improvement on the NWP turbulent fluxes.

6. Summary and Discussion

RAMA addresses a long standing need for a sustained moored buoy array in the Indian Ocean for climate studies. It will take several years to complete and will require coordinated resource contributions (financial, human, and ship time) from several countries. Implementation of RAMA will result in a globe girdling network of tropical moored buoy arrays that includes TAO/TRITON in the Pacific and PIRATA in the Atlantic. Like these other arrays, we can expect that RAMA will fundamentally contribute to research by enabling advances in our understanding of large scale ocean dynamics, ocean-atmosphere interactions, and climate variability in the Indian Ocean region.

We can also expect that RAMA will contribute to operational activities as a component of GOOS, the Global Climate Observing System (GCOS), and the Global Earth Observing System of Systems (GEOSS). Indeed, real-time RAMA data are already being incorporated into weather forecasts and seasonal climate forecasts produced by operational centers. RAMA can likewise provide valuable data for operational ocean state estimation and for oceanic and atmospheric reanalysis products. Finally, the data will find uses for satellite validation and for the validation of oceanic and atmospheric dynamical models.

RAMA moorings, and in particular those specially instrumented reference sites for air-sea heat, moisture and momentum fluxes, are a contribution to the Ocean Sustained Interdisciplinary Timeseries Environment observation System (OceanSITES),

500 a worldwide network of deep water stations providing high temporal resolution data for
501 ocean research and environmental forecasting (http://www.oceansites.org/). In addition,
502 RAMA is capable of accommodating biogeochemical sensors to support programs such
503 as the International Ocean Carbon Coordination Project (IOCCP; http://www.ioccp.org/)
504 and the Sustained Indian Ocean Biogeochemical and Ecological Research (SIBER)
505 program (Hood et al, 2008). RAMA will provide information on oceanic variability of
506 value to the Joint Aerosol-Monsoon Experiment (JAMEX; Lau et al, 2008), which is a
507 multi-national study scheduled for 2007-11 to investigate the effects of aerosols on
508 ocean-atmosphere-land interactions that govern the Asian monsoon water cycle. In the
509 wake of the December 2004 Asian tsunami, discussions are also underway with
510 organizations involved in developing the Indian Ocean tsunami warning system on how
511 best to coordinate implementation efforts with IndOOS. A joint RAMA and tsunami
512 mooring cruise has already been conducted aboard the Indonesian Research Vessel
513 Baruna Jaya III in September 2007
514 (http://www.noaanews.noaa.gov/stories2007/s2919.htm). In the longer term, it may
515 beneficial to consider development of a multi-hazard moored buoy platform for both
516 tsunami warnings and climate studies.

517 RAMA will provide a long-term, broad scale spatial and temporal context for
518 short duration, geographically focused process studies. Examples include the Mirai
519 Indian Ocean cruise for the Study of the MJO convection Onset (MISMO; Yoneyama et
520 al, 2008), which took place in October-December 2006 around 0°, 80.5°E, and the
521 French-lead VASCO-Cirene project (Duvel et al, 2008; Vialard et al, 2008a) which took
522 place in the Seychelles-Chagos thermocline ridge region of the southwest Indian Ocean

523 in January-February 2007. Both these process studies examined ocean-atmosphere
524 interactions associated with the MJO for which the high resolution moored time series
525 data are especially valuable (e.g. Vialard et al, 2008b). The moored array in turn will
526 benefit from process studies, since new knowledge gained from programs like MISMO
527 and VASCO-Cirene can feedback into design specifications for RAMA. Moreover, the
528 VASCO-Cirene field campaign provided the opportunity to deploy a flux reference site
529 mooring at 8°S, 67°E.

530 In summary, full implementation of RAMA promises significant scientific and
531 societal benefits. There are major challenges, however, not only in identifying and
532 securing the necessary resources to complete the array, but in forging long-lasting multi-
533 national partnerships to sustain it into the future. We know that success is possible
534 though because it has been achieved in the past for similar mooring programs of
535 ambitious scope in the tropical Pacific and Atlantic.

536

Acknowledgments

The authors would like to thank the International CLIVAR Project Office and the Intergovernmental Oceanographic Commission Perth Regional Office for supporting the Indian Ocean Panel. We also wish to acknowledge the many institutions and organizations that have contributed to the implementation of RAMA: in India, the Ministry of Earth Sciences, the National Center for Antarctic and Ocean Research, the Indian National Center for Ocean Information Services and the National Institute of Oceanography; in Japan, the Japan Agency for Marine-Earth Science and Technology and the Ministry of Education, Sports, Culture, Science and Technology; in China, the State Oceanic Administration, First Institute of Oceanography, and Ministry of Science and Technology; in Indonesia, the Agency for the Assessment and Application of Technology and the Agency for Marine and Fisheries Research; and the U.S., the NOAA Climate Program Office and the TAO Project Office of NOAA/PMEL. This manuscript was initiated while the first author was a guest at the University of Tasmania's Integrated Marine Observing System Office in Hobart, Australia. PMEL publication number 3199 and NIO contribution number XXXX. This paper is dedicated to the memory of our friend and colleague Fritz Schott, who inspired us through his scientific leadership, wise counsel, and deep understanding of the ocean.

554 References

555 Alory, G., S. Wijffels, and G. Meyers (2007), Observed temperature trends in the Indian
556 Ocean over 1960—1999 and associated mechanisms, Geophys. Res. Lett., 34, L02606,
557 doi:10.1029/2006GL028044.

558 Annamalai H., and R. Murtugudde, 2004: Role of the Indian Ocean in regional climate
559 variability. Earth's Climate: The Ocean-Atmosphere Interaction, Geophys. Monogr., No.
560 147, Amer. Geophys. Union, 213–246.
561
562 Annamalai, H., H. Okajima, and M. Watanabe, 2007: Possible Impact of the Indian
563 Ocean SST on the Northern Hemisphere Circulation during El Niño. J. Climate, 20,
564 3164–3189.
565
566 Arguez, A., 2007: Supplement to State of the Climate in 2006. Bull. Amer. Meteor. Soc.,
567 88, s1–s135.
568
569 Ashok K., W.-L. Chan, T. Motoi, T. Yamagata, 2004: Decadal variability of the Indian
570 Ocean dipole, Geophys. Res. Lett., 31, L24207, doi:10.1029/2004GL021345.
571
572 Bessafi, M. and M.C. Wheeler, 2006: Modulation of south Indian ocean tropical cyclones
573 by the Madden-Julian oscillation and convectively coupled equatorial waves, Mon. Wea.
574 Rev., 134, 638-656.
575
576 Bhat, G. S., S. Gadgil, P.V. Hareesh Kumar, S. R. Kalsi, P. Madhusoodanan, V. S. N.
577 Murty, C. V. K. Prasada Rao, V. Ramesh Babu, L. V. G. Rao, R. R. Rao, M.
578 Ravichandran, K. G. Reddy, P. Sanjeeva Rao, D. Sengupta, D. R. Sikka, J. Swain, and P.
579 N. Vinayachandran, 2001: BOBMEX: The Bay of Bengal Monsoon Experiment. *Bull.*
580 *Am. Meteorol. Soc.*, 82, 2217-2243.
581
582 Bonjean, F. and Lagerloef, G. E. S.: Diagnostic Model and Analysis of the Surface
583 Currents in the Tropical Pacific Ocean, 2002: J. Phys. Oceanogr., 32, 2938–2954, 2002.
584
585 Bourlès, B., R. Lumpkin, M. J. McPhaden, F. Hernandez, P. Nobre, E. Campos, L. Yu, S.
586 Planton, A. J. Busalacchi, A. D. Moura, J. Servain, and J. Trotte, 2008: The PIRATA
587 Program: History, Accomplishments, and Future Directions. *Bull. Amer. Meteorol. Soc.,*
588 in press.
589
590 Cherchi, A., S. Gualdi, S. Behera, J. J. Luo, S. Masson, T. Yamagata, and A. Navarra,
591 2007: The Influence of Tropical Indian Ocean SST on the Indian Summer Monsoon. J.
592 Climate, 20, 3083–3105.
593
594 Clark, C.O., J. E. Cole, and P. J. Webster, 2000: Indian Ocean SST and Indian Summer
595 Rainfall: Predictive Relationships and Their Decadal Variability. J. Climate, 13, 2503–
596 2519.
597

598 CLIVAR-GOOS Indian Ocean Panel, 2006: Understanding the role of the Indian Ocean
599 in the climate system - Implementation Plan for sustained observations. ICPO Publication
600 Series #100, International CLIVAR Project Office, Southampton, UK, 76pp.
601
602 de Ruijter, W. P. M., A. Biastoch, S. S. Drijfhout, J. R. E. Lutjeharms, R. P. Matano, T.
603 Pichevin, P. J. van Leeuwen, and W. Weijer, 1999: Indian-Atlantic interocean exchange:
604 Dynamics, estimation and impact, J. Geophys. Res., 104(C9), 20,885–20,910.
605
606 Duvel, J.P., and J. Vialard, 2007: Indo-Pacific Sea Surface Temperature Perturbations
607 Associated with Intraseasonal Oscillations of Tropical Convection. J. Climate, 20, 3056–
608 3082.
609
610 Duvel, J-P., C. Basdevant, H. Bellenger, G. Reverdin, A. Vargas and J. Vialard, 2008:
611 The Aeroclipper: A new device to explore convective systems and cyclones, *Bull. Am.*
612 *Met. Soc*, in press.
613
614 ECMWF, 1994: The description of the ECMWF/WCRP level III-A atmospheric data
615 archive. Technical Attachment, ECMWF Shinfield Park, Reading, UK, 72pp.
616
617 Fairall, C. F., E. F. Bradley, J. E. Hare, A. A. Grachev, and J. B. Edson, 2003: Bulk
618 parameterization of air-sea fluxes: Updates and verification for the COARE algorithm, *J.*
619 *Climate*, 16, 571–591.
620
621 Feng, M., G. Meyers, and S. Wijffels, 2001: Interannual Upper Ocean Variability in the
622 Tropical Indian Ocean, Geophys. Res. Lett., 28(21), 4151–4154.
623
624 Fu, L.L., 2007: Intraseasonal Variability of the Equatorial Indian Ocean Observed from
625 Sea Surface Height, Wind, and Temperature Data. J. Phys. Oceanogr., 37, 188–202.
626
627 Giannini, A., R. Saravanan, and P. Chang, 2003: Oceanic forcing of Sahel rainfall on
628 interannual to interdecadal time scales, Science, 302, 1027–1030.
629
630 Gordon, A. L., 2001: Interocean exchange. In: Ocean Circulation and Climate, G. Siedler,
631 J. Church and J. Gould (eds.), Academic Press, pp. 303-314.
632
633 Han, W., P. Webster, R. Lukas, P. Hacker, and A. Hu, 2004: Impact of Atmospheric
634 Intraseasonal Variability in the Indian Ocean: Low-Frequency Rectification in Equatorial
635 Surface Current and Transport. J. Phys. Oceanogr., 34, 1350–1372.
636
637 Han, W., 2005: Origins and Dynamics of the 90-Day and 30–60-Day Variations in the
638 Equatorial Indian Ocean. J. Phys. Oceanogr., 35, 708–728.
639
640 Harrison, D. E., and M. Carson, 2007: Is the World Ocean Warming? Upper-Ocean
641 Temperature Trends: 1950–2000. J. Phys. Oceanogr., 37, 174–187.
642
643 Hase, H., Y. Masumoto, Y. Kuroda, and K. Mizuno, 2008: Semiannual variability in

644 temperature and salinity observed by Triangle Trans-Ocean Buoy Network (TRITON)
645 buoys in the eastern tropical Indian Ocean, J. Geophys. Res., 113, C01016,
646 doi:10.1029/2006JC004026.
647
648 Hermes, J. C. and C. J. C. Reason, 2008: Annual cycle of the South Indian Ocean
649 (Seychelles-Chagos) thermocline ridge in a regional ocean model. J. Geophys. Res.,
650 doi:10.1029/2007JC004363, in press.
651
652 Higgins, R.W., and K.C. Mo, 1997: Persistent North Pacific Circulation Anomalies and
653 the Tropical Intraseasonal Oscillation. J. Climate, 10, 223–244.
654
655 Hoerling, M. P., J. W. Hurrell, and T. Xu, 2001: Tropical Origins for Recent North
656 Atlantic Climate Change. Science, 292, 90-92.
657
658 Hoerling, M., and A. Kumar, 2003: The perfect ocean for drought, Science, 299, 691–
659 694.
660
661 Hood, R. R., A. Naqvi, J. D. Wiggert, J. Goes, V.Coles, J. McCreary, N. Bates, P. K.
662 Karuppasamy, N. Mahowald, S. Seitzinger, and G. Meyers, 2008: Research opportunities
663 and challanges in the Indian Ocean. Eos Trans. AGU, 89(13), 125-26.
664
665 Izumo, T., C. de Boyer Montegut, J-J. Luo, S.K. Behera, S. Masson and T. Yamagata,
666 2008: The role of the western Arabian Sea upwelling in Indian monsoon rainfall
667 variability, J. Climate, accepted.
668
669 Janowiak, J. E. and Xie, P., 1999: CAMS OPI: A Global Satellite-Rain Gauge Merged
670 Product for Real-Time Precipitation Monitoring Applications, J. Climate, 12, 3335–3342.
671
672 Josey, S. A., E. C. Kent, and P. K. Taylor, 1999: New insights into the ocean heat budget
673 closure problem from analysis of the SOC air–sea flux climatology. J. Climate, 12, 2850–
674 2880.
675
676 Kalnay, E., and Coauthors, 1996: The NCEP/NCAR 40-Year Reanalysis Project. Bull.
677 Amer. Meteor. Soc., **77,** 437–471.
678
679 Kanamitsu, M., W. Ebisuzaki, J. Woolen, J. Potter, S-K Yang, J.J. Hnilo, M. Fiorino, and
680 G. L. Potter, 2002: NCEP-DEO AMIP-II Reanalysis (R-2). Bull. Atmos. Met. Soc., **83,**
681 1631–1643.
682
683 Knauss, J. A., 1961: The International Indian Ocean Expedition. Science, 134, 1674-
684 1676.
685
686 Knox, R. A., 1976: On a long series of measurements of Indian Ocean equatorial currents
687 near Addu Atoll. Deep-Sea Res., 23, 211-222.
688

689 Kuroda Y. and Y. Amitani, 2000: TRITON--New ocean and atmospheric observing buoy
690 network for monitoring ENSO, Umi no Kenkyu, 10, 157-172.
691
692 Krishnamurti, T., 1985: Summer Monsoon Experiment—A Review. Mon. Wea.
693 Rev., 113, 1590–1626.
694
695 Lau, K.-M. and Co-authors, 2008: The joint aerosol-monsoon experiment: A new
696 challenge for monsoon climate research. Bull. Am. Meteorol. Soc., 89. 369-381.
697 Lee, T. and M.J. McPhaden, 2008: Decadal phase change in large-scale sea level and
698 winds in the Indo-Pacific region at the end of the 20th century. Geophys. Res. Lett., 35,
699 L01605, doi:10.1029/2007GL032419.
700
701 Levitus, S., J. Antonov, and T. Boyer, 2005: Warming of the world ocean, 1955 – 2003,
702 Geophys. Res. Lett., 32, L02604, doi:10.1029/ 2004GL021592.
703
704 Liebmann, B., H. H. Hendon and J. D. Glick, 1994: The Relationship between tropical
705 cyclone of the Western Pacific and Indian Oceans and the Madden-Julian Oscillation, J.
706 Met. Soc. Jap., 72, 401-412.
707
708 Luo, J. J., S. Masson, S. Behera, and T. Yamagata, 2007: Experimental Forecasts of the
709 Indian Ocean Dipole Using a Coupled OAGCM. J. Climate, 20, 2178–2190.
710 Luyten, J. R., M. Fieux, and J. Gonella, 1980: Equatorial currents in the western Indian
711 Ocean. Science, 209, 600-603.
712
713 Luyten, J.R., and D.H. Roemmich, 1982: Equatorial Currents at Semi-Annual Period in
714 the Indian Ocean. J. Phys. Oceanogr., 12, 406–413.
715
716 Madden, R.A., and P.R. Julian, 1994: Observations of the 40–50-Day Tropical
717 Oscillation—A Review. Mon. Wea. Rev., 122, 814–837.
718
719 Maloney, E.D., and D.L. Hartmann, 2000: Modulation of Eastern North Pacific
720 Hurricanes by the Madden–Julian Oscillation. J. Climate, 13, 1451–1460.
721
722 Masumoto, Y., H. Hase, Y. Kuroda, H. Matsuura, and K. Takeuchi, 2005: Intraseasonal
723 variability in the upper layer currents observed in the eastern equatorial Indian Ocean.
724 *Geophys. Res. Lett.,* **32**, L02607, doi:10.1029/2004GL021896.
725
726 McPhaden, M. J., 1999: Genesis and evolution of the 1997–98 El Niño, Science, 283,
727 950–954.
728
729 McPhaden, M. J., A. J. Busalacchi, R. Cheney, J. R. Donguy, K. S. Gage, D. Halpern, M.
730 Ji, P. Julian, G. Meyers, G. T. Mitchum, P. P. Niiler, J. Picaut, R. W. Reynolds, N. Smith,
731 K. Takeuchi, 1998: The Tropical Ocean-Global Atmosphere (TOGA) observing system:
732 A decade of progress. J. Geophys. Res., 103, 14,169-14,240.
733
734 McPhaden M. J., Y. Kuroda, and V. S. N. Murty, 2006: Development of an Indian Ocean

735 Moored Buoy Array for Climate Studies. CLIVAR Exchanges, 11(4), International
736 CLIVAR Project Office, Southampton, UK, p. 3-5.
737
738 Meyers, G. and R. Boscolo, 2006: The Indian Ocean Observing System (IndOOS).
739 CLIVAR Exchanges, 11(4), International CLIVAR Project Office, Southampton, UK, p.
740 2-3.
741
742 Murty, V. S. N., M.S.S. Sarma, A. Suryanarayana, D. Sengupta, A. S. Unnikrishnan,V.
743 Fernando, A. Almeida, S. Khalap, A. Sardar, K. Somasundar, and M. Ravichandran,
744 2006: Indian Moorings: Deep-sea current meter moorings in the Eastern Equatorial
745 Indian Ocean. CLIVAR Exchanges, 11(4), International CLIVAR Project Office,
746 Southampton, UK, p. 5-8.
747
748 Murty, V.S.N., Bulusu Subrahmanyam, S. Muralikrishna, David M. Heffner, A.S.N.
749 Lakshmi, C. Neelima and P. J. Vidya, 2008: Seasonal and Interannual Variability of Sea
750 Surface Salinity during 2002-06 from Argo profiles and OGCM simulations in the
751 tropical Indian Ocean. J. Geophys. Res., in revision.
752
753 National Research Council, 1996: Learning to predict climate variations associated with
754 El Niño and the southern oscillation. Accomplishments and legacies of the TOGA
755 Program. National Academy Press, Washington, D.C., 171 pp.
756 National Research Council, 2000: Fifty Years of Discovery: National Science Foundation
757 1950-2000. National Academy Press, Washington, DC, 270 pp.
758
759 Oke, P. R., and A. Schiller, 2007: A Model-Based Assessment and Design of a Tropical
760 Indian Ocean Mooring Array. J. Climate, 20, 3269–3283.
761
762 Reppin, J., F. Schott, J. Fishcher, and D. Quadfasel, 1999: Equatorial currents and
763 transports in the upper central Indian Ocean. *J. Geophys. Res*., **104**, 15495-15514.
764
765 Reynolds, R. W., Rayner, N. A., Smith, T. M., Stokes, D. C., and Wang, W. Q., 2002: An
766 improved in situ and satellite SST analysis for climate, J. Climate, 15, 1609–1625.
767
768 Rudnick, D. L., R. A. Weller, C. C. Eriksen, T. D. Dickey, J. Marra, and C. Langdon,
769 1997: Moored instruments weather Arabian Sea monsoons, yield data. EOS, *Trans. Am.*
770 *Geophys. Union* **78**, 117, 120-121.
771
772 Saji, N. H., B. N. Goswami, P. N. Vinayachandran and T. Yamagata, 1999: A dipole
773 mode in the tropical Indian Ocean. *Nature,* **401,** 360-363.
774
775 Sanjeeva Rao, P. and D. R. Sikka, 2005: Intraseasonal Variability of the summer
776 monsoon over the North Indian Ocean as revealed by the BOBMEX and ARMEX field
777 Programs, Pure Appl. Geophys. 162, 1481–1510.
778
779 Schott, F., and J. P. McCreary, 2001: The monsoon circulation of the Indian Ocean, Prog.
780 Oceanogr., 51, 1-123.

781
782 Schott, F. A., J. P. McCreary, and G. C. Johnson, 2004: Shallow over-turning circulations
783 of the tropical-subtropical oceans. In Earth Climate: The Ocean-Atmosphere Interaction.
784 C. Wang, S.-P. Xie, and J. Carton (eds.), *Geophys. Monograph,* **147**, AGU, Washington,
785 D.C., p. 261-304.
786
787 Schott, F. A., S.-P. Xie, and J. P. McCreary, 2008: Indian Ocean circulation and climate
788 variability. Rev. Geophys., submitted.
789
790 Seiki, A., and Y.N. Takayabu, 2007: Westerly Wind Bursts and Their Relationship with
791 Intraseasonal Variations and ENSO. Part I: Statistics. Mon. Wea. Rev., 135, 3325–3345.
792
793 Sengupta, D., R. Senan, B.N. Goswami and J. Vialard, 2007: Intraseasonal variability of
794 equatorial Indian Ocean zonal currents, *Journal of Climate,* **20,** 3036-3055.
795
796 Sengupta, D., R. Senan, V. S. N. Murty, and V. Fernando, 2004: A biweekly mode in the
797 equatorial Indian Ocean. *J. Geophys. Res.,* **109,** C10003, doi:10.1029/2004JC002329.
798
799 Shinoda, T., and W. Han, 2005: Influence of the Indian Ocean Dipole on Atmospheric
800 Subseasonal Variability. J. Climate, 18, 3891–3909.
801
802 Shenoi, S. S. C., D. Shankar, and S. R. Shetye, 2002: Differences in heat budgets of the
803 near surface Arabian Sea and Bay of Bengal: Implications for the summer monsoon,
804 *Journal of Geophysical Research*, *107*, C6, 10.1029/2000JC000679.
805
806 Siedler, G., J. Church and J. Gould (eds.), 2001: Ocean Circulation and Climate -
807 Observing and Modelling the Global Ocean. Academic Press, San Diego, 715pp.
808
809 Slingo, J. M., et al., 1996: Intraseasonal oscillations in 15 atmospheric general circulation
810 models: Results from an AMIP diagnostic subproject, Clim. Dyn., 12, 325–357.
811
812 Smith, S. L., 2001: Understanding the Arabian Sea: Reflections on the 1994–1996
813 Arabian Sea Expedition. Deep-Sea Res. Part II: Topical Studies in Oceanography, 48,
814 1385-1402.
815
816 Syamsudin, F., A. Kaneko, and D. B. Haidvogel, 2004: Numerical and observational
817 estimates of Indian Ocean Kelvin wave intrusion into Lombok Strait. Geophys. Res.
818 Lett., L24307, doi:10.1029/2004GL021227.
819
820 Taft, B. A. and J. A. Knauss, 1967: The equatorial undercurrent in the Indian Ocean as
821 observed by the Lusiad Expedition. Bull. Scripps Inst. Oceanogr., 9, 163pp.
822
823 Uppala, S., and Coauthors, 2005: The ERA-40 re-analysis. Quart. J. Roy. Meteor. Soc.,
824 **131,** 2961–3012.
825
826 Vecchi, G.A. and D.E. Harrison, 2004: Interannual Indian rainfall variability and Indian

827 Ocean sea surface temperature anomalies. In *Earth Climate: The Ocean-Atmosphere*
828 *Interaction,* C. Wang, S.-P. Xie, and J.A. Carton (eds.), American Geophysical Union,
829 Geophysical Monograph 147, Washington D.C., 247-260.
830
831 Vecchi, G.A., and M.J. Harrison, 2007: An Observing System Simulation Experiment for
832 the Indian Ocean. J. Climate, 20, 3300–3319.
833
834 Vialard, J., J.P. Duvel, M. McPhaden, P. Bouruet-Aubertot, B. Ward, E. Key, D. Bourras,
835 R. Weller, P. Minnett, A. Weill, C. Cassou, L. Eymard, T. Fristedt, C. Basdevant, Y.
836 Dandoneau, O. Duteil, T. Izumo, C. de Boyer Montégut, S. Masson1, F. Marsac, 2008a:
837 Cirene: Air-sea interactions in the Seychelles-Chagos thermocline ridge region. Bull.
838 Am. Meteorol. Soc., submitted.
839
840 Vialard, J., G. Foltz, M. McPhaden, J.P. Duvel, and C. de Boyer Montégut, 2008b:
841 Strong Indian Ocean cooling driven by the Madden-Julian oscillation in late 2007 and
842 early 2008. Geophys. Res. Lett., submitted.
843
844 Wainwright, L., G. Meyers, S.Wijffels, and L. Pigot, 2008: Change in the Indonesian
845 Throughflow with the climate shift of 1966/77. Geophys. Res. Lett., L03604,
846 doi:10.1029/2007GL031911.
847
848 Waliser D. E., K.-M. Lau, and J.-H. Kim, 1999: The Influence of Coupled Sea Surface
849 Temperatures on the Madden-Julian Oscillation: A ModelPerturbation Experiment. J.
850 Atmos. Sci., 56, 333-358.
851
852 Wajsowicz, R. C., 2005: Potential predictability of tropical Indian Ocean SST anomalies,
853 Geophys. Res. Lett., 32, L24702, doi:10.1029/2005GL024169.
854
855 Waple, A. M., and J. H. Lawrimore, 2003: State of the Climate in 2002. Bull. Amer.
856 Meteor. Soc., 84, 800.
857
858 Webster, P. W., A. M. Moore, J. P. Loschnigg and R. R. Lebben, 1999: Coupled ocean-
859 atmosphere dynamics in the Indian Ocean during 1997-98, *Nature*, **401**, 356-360.
860
861 Webster, P. J., E. F. Bradley, C. W. Fairall, J. S. Godfray, P. Hacker, R. A. Houze Jr., R.
862 Lukas, Y. Serra, J. M. Hummon, T. D. M. Lawrence, C. A. Russell, M. N. Ryan, K.
863 Sahami, and P. Zuidema, 2002: The JASMINE pilot study. Bull. Am. Meteorol. Soc., 83,
864 1603-1630.
865
866 Webster, P. J, and C. Hoyos, 2004: Prediction of Monsoon Rainfall and River Discharge
867 on 15-30 day Time Scales. Bull. Am. Meteorol. Soc., 85, 1745-1765.
868
869 Wijffels, S. and G. Meyers, 2004: An intersection of oceanic waveguides—variability in
870 the Indonesian throughflow region. *J. Phys. Oceanogr.* **34**, 1232-1253.
871
872 Woolnough S. J., F. Vitart, and M. Balmaseda, 2007: The role of the ocean in the

Madden-Julian Oscillation: Sensitivity of an MJO forecast to ocean coupling. Quart. J. Roy. Meteor. Soc., 133, 117–128.

Xie, S.P., H. Annamalai, F. A. Schott, and J. P. McCreary, 2002: Structure and Mechanisms of South Indian Ocean Climate Variability. J. Climate, 15, 864–878.

Yang, J., Q. Liu, S.-P. Xie, Z. Liu, and L. Wu, 2007: Impact of the Indian Ocean SST basin mode on the Asian summer monsoon, Geophys. Res. Lett., 34, L02708, doi:10.1029/2006GL028571.

Yaremchuk, M., 2006: Sea surface salinity constrains rainfall estimates over tropical oceans, Geophys. Res. Lett., 33, L15605, doi:10.1029/2006GL026582.

Yokoi, T., T. Tozuka and T. Yamagata, 2008: Seasonal variation of the Seychelles Dome. J. Clim., in press.

Yu, W., B. Xiang, L. Liu, and N. Liu, 2005: Understanding the origins of interannual thermocline variations in the tropical Indian Ocean. Geophys. Res. Lett., 32, L24706, doi:10.1029/2005GL024327.

Yu, L., X. Jin, and R.A. Weller, 2007: Annual, Seasonal, and Interannual Variability of Air–Sea Heat Fluxes in the Indian Ocean. J. Climate, 20, 3190–3209.

Yu, L., and R.A. Weller, 2007: Objectively Analyzed Air–Sea Heat Fluxes for the Global Ice-Free Oceans (1981–2005). Bull. Amer. Meteor. Soc., 88, 527–539.

Yu, Z., and J. P. McCreary Jr., 2004; Assessing precipitation products in the Indian Ocean using an ocean model, J. Geophys. Res., 109, C05013, doi:10.1029/2003JC002106.

Zhang, C., 2005: Madden-Julian Oscillation, Rev. Geophys., 43, RG2003, doi:10.1029/2004RG000158.

Zhang, Y., W. B. Rossow, A. A. Lacis, V. Oinas, and M. I. Mishchenko, 2004: Calculation of radiative fluxes from the surface to top of atmosphere based on ISCCP and other global data sets: Refinements of the radiative transfer model and the input data, J. Geophys. Res., 109, D19105, doi:10.1029/2003JD004457.

SIDE BOX 1: RAMA moorings

Four types of moorings are presently used in RAMA. Most of the surface moorings at present are Next Generation ATLAS mooring supplied by NOAA's Pacific Marine Environmental Laboratory (PMEL). These taut line surface moorings are anchored to the ocean floor in depths of typically 2500-5000 m. Measurements on the surface float include air temperature, relative humidity, wind velocity, downwelling shortwave radiation, rain rate, and sea surface temperature and salinity (the latter two nominally at 1 m depth). Sensors on the mooring line measure ocean temperature (12 depths between 10 m and 500 m), salinity (5 depths between 10 m and 100 m), mixed layer velocity (at 10 m depth) and pressure (at depths of 300 m and 500 m). Flux reference site moorings include sensors for downwelling longwave radiation and barometric pressure, as well as additional sensors in the upper 140 m of the ocean for temperature, salinity and velocity. . Daily averages of all data and several hourly samples per day of most meteorological variables are transmitted to shore in real-time via Service Argos. These data are placed on the Global Telecommunications System (GTS) for use in operational weather, climate, and ocean forecasting. Higher temporal resolution data (at 1- to 10-minute intervals in most cases) are internally recorded and available after mooring recovery. More information on ATLAS moorings can be found at http://www.pmel.noaa.gov/tao/proj_over/mooring.shtml .

TRITON moorings, supplied by Japan Marine-Earth Science and Technology Agency (JAMSTEC), are presently deployed at 1.5°S, 90°E and 5°S, 95°E. TRITON moorings were designed specifically to be functionally equivalent to ATLAS moorings in terms of sensor payloads, temporal resolution, and data accuracy. There are some

933 differences (e.g. TRITON moorings are deployed with more salinity sensors,
934 measurements are made to 750 m rather than 500 m, and hourly rather than daily
935 averages of all data are transmitted to shore in real-time), but these differences do not
936 affect comparability of the basic data sets. More information on TRITON moorings can
937 be found at http://www.jamstec.go.jp/jamstec/TRITON/real_time/overview.php/po.php .
938 Acoustic Doppler Current Profile (ADCP) moorings, deployed at several
939 locations in the array, measure velocity from profilers mounted in a subsurface float
940 typically located at depths 300-400 m below the surface. The ADCP is positioned with
941 its acoustic beams pointing upward, measuring profiles of velocity at typically hourly
942 intervals with ~10 m vertical resolution. Backscatter from the ocean surface interferes
943 with velocity retrievals in the upper 30-40 m of the water column, so subsurface ADCPs
944 do not measure effectively in this depth range (hence the need for current meters in the
945 mixed layer on the surface moorings). ADCP data are available upon mooring recovery.
946 Deep ocean moorings maintained by India's National Institute of Oceanography
947 (NIO) have a subsurface float at 100-200 m depth, below which 6 mechanical current
948 meters are attached to the mooring line for velocity measurements down to a depth of
949 approximately 4000 m. Beginning in 2003, upward-pointing ADCPs were added to the
950 near surface float additional velocity measurements. Data from these moorings is
951 available on recovery. More information on these moorings is available from Murty et al
952 (2006).
953 A web portal with pointers to data from all moorings is found at
954 http://www.incois.gov.in/Incois/iogoos/home_indoos.jsp . Subsets of the data are
955 available from http://www.pmel.noaa.gov/tao/ (ATLAS, TRITON, ADCP),

http://www.jamstec.go.jp/ (TRITON and JAMSTEC ADCP), and

http://www.nio.org/data_info/deep-sea_mooring/oos-deep-sea-currentmeter-moorings.htm (NIO deep ocean moorings).

SIDE BOX 2: RAMA Implementation Time Line

RAMA traces its roots to Indian and Japanese national efforts initiated in 2000. JAMSTEC deployed an ADCP mooring at 0°, 90°E in 2000 (Masumoto et al, 2005) and two TRITON moorings at 1.5°S, 90°E and 5°S, 95°E in 2001 (Hase et al, 2008). NIO also began subsurface mooring deployments to sample the deep ocean along the equator in 2000 (Sengupta et al, 2004; Murty et al, 2006). These efforts, which have continued without interruption, were precursors to RAMA and incorporated into the array design. Then, in October-November 2004, NOAA/PMEL in collaboration with NIO and the Indian Ministry of Earth Sciences (MoES) deployed four ATLAS moorings and one ADCP mooring near the equator between 80°-90°E. PMEL and the Indonesian Agency for the Assessment and Application of Technology (BPPT) and the Ministry for Marine Affairs and Fisheries (DKP) occupied sites at 4°N, 90°E and 8°N, 89°E in November 2006. An ATLAS mooring was deployed in the southwest Indian Ocean at 8°S, 67°E as part of the French-lead VASCO-Cirene experiment in January 2007 (Duvel et al, 2008; Vialard et al, 2008a) while in November 2007 a Chinese ADCP mooring was deployed off the coast of Java as part of a collaboration between the Chinese First Institute of Oceanography (FIO), BPPT, and DKP. Also in November 2007, PMEL and Indian technicians deployed two ATLAS moorings in the Bay of Bengal (12°N and 15°N, 90°E) on a cruise lead by the Indian National Center for Ocean Information Services (INCOIS). These efforts to build the array will continue, with the expectation that the mooring array will be completed within the next several years.

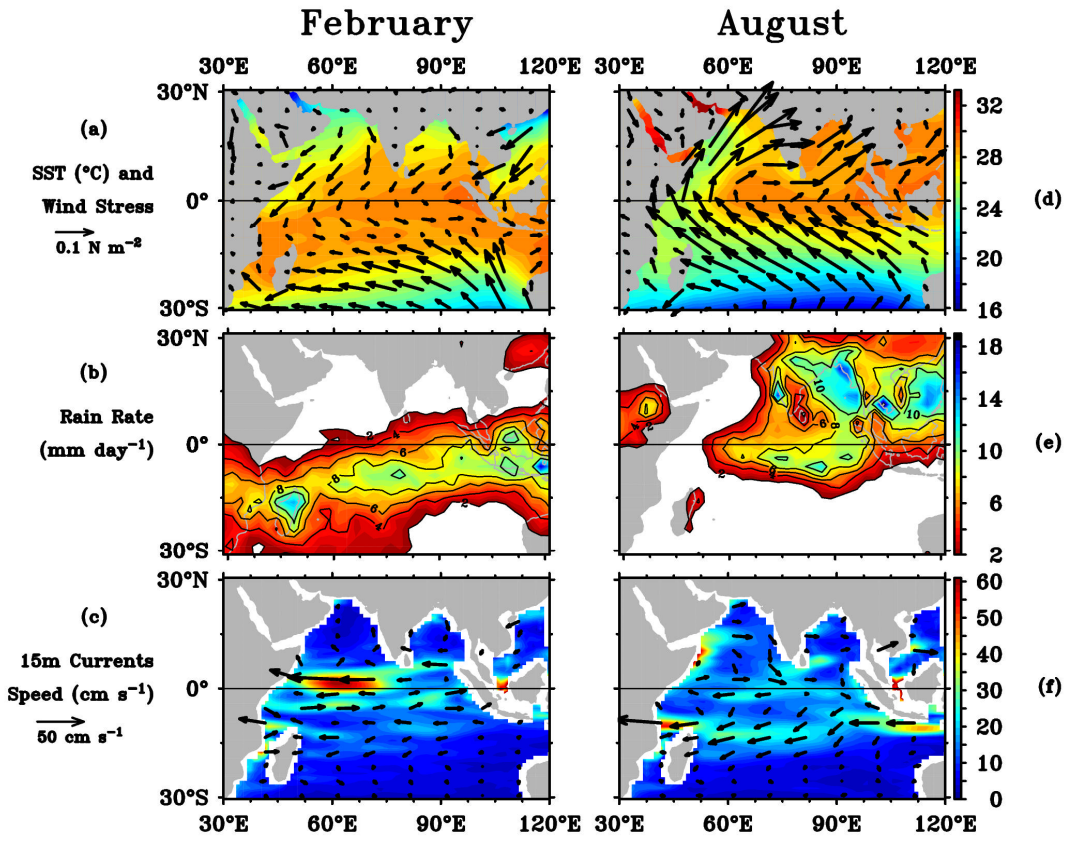

Figure 1. Seasonal means for December-February of (a) surface wind stress (in N m^{-2}) and SST (in °C); (b) rain rate (in mm day^{-1}); and (c) current velocity (vectors) and speeds (color shading) representative of flow at 15 m depth in the surface mixed layer (in cm s^{-1}). Corresponding seasonal means for June-August are in (d)-(f). SSTs are based on Reynolds et al. (2002), winds are from the ECMWF-ERA40 reanalysis dataset (http://data.ecmwf.int/data/d/era40_daily/), currents are from Bonjean and Lagerloef (2002), and rain rate is from an analysis of satellite and in situ raingauge data (Janowiak and Xie, 1999). The current analysis in (c) and (f) does not extend to the coasts and so does not show western boundary currents like the Somali Current. Rain rate is contoured for values ≥ 2 mm day^{-1}.

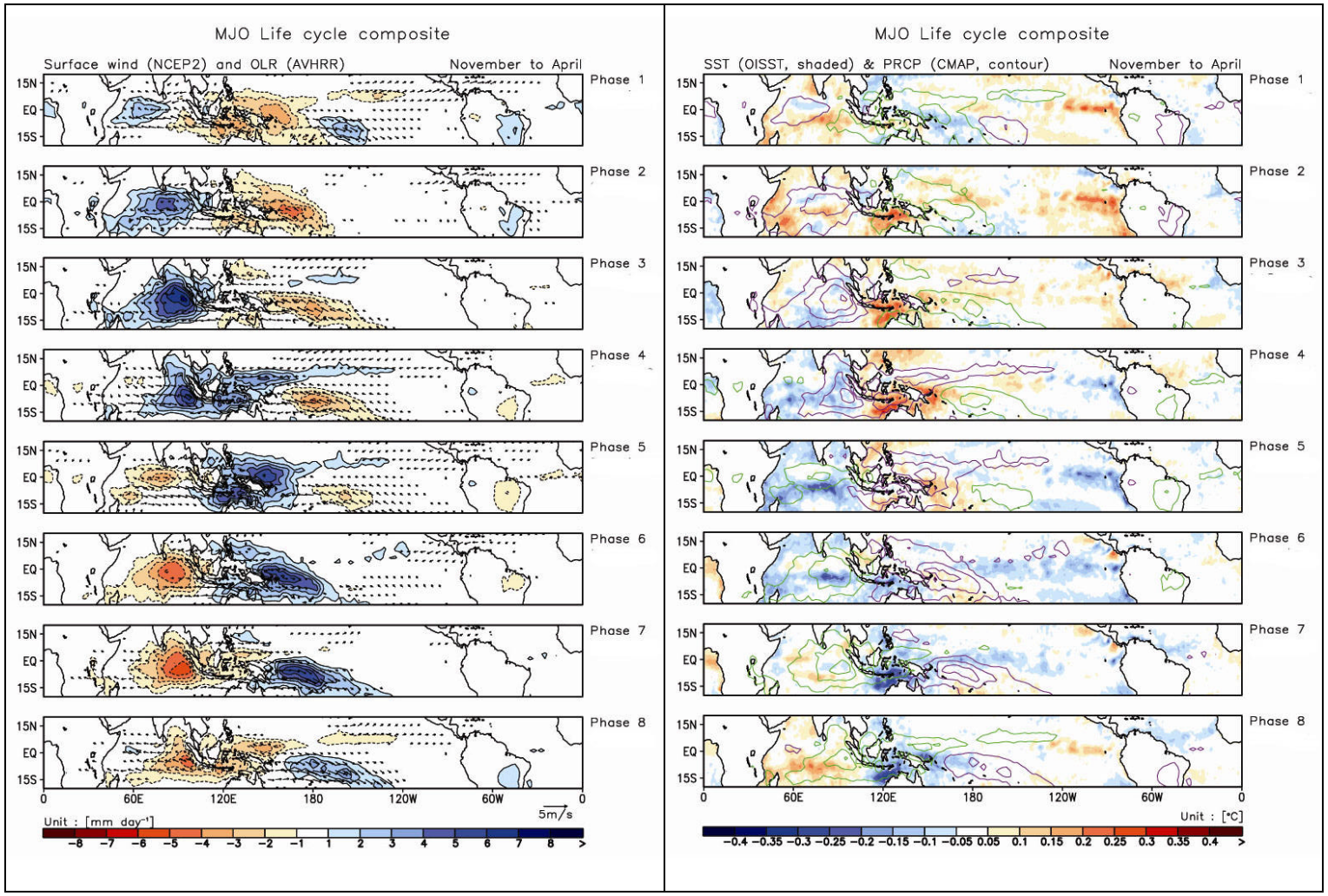

Figure 2. Left panels: Composite of band-pass filtered (20-100 day periods) November-April Outgoing Longwave Radiation (OLR) (color) and the National Centers for Environmental Prediction NCEP1surface wind anomalies (vectors) as a function of MJO phase. Zonal wind anomalies statistically significant at 99% based on Student's t test are drawn. The reference vector in units of m $s^{-1}$is s hown at the bottom right. Right panels: same as left panels, but for SST and rainrate (courtesy of US MJO CLIVAR Working Group).

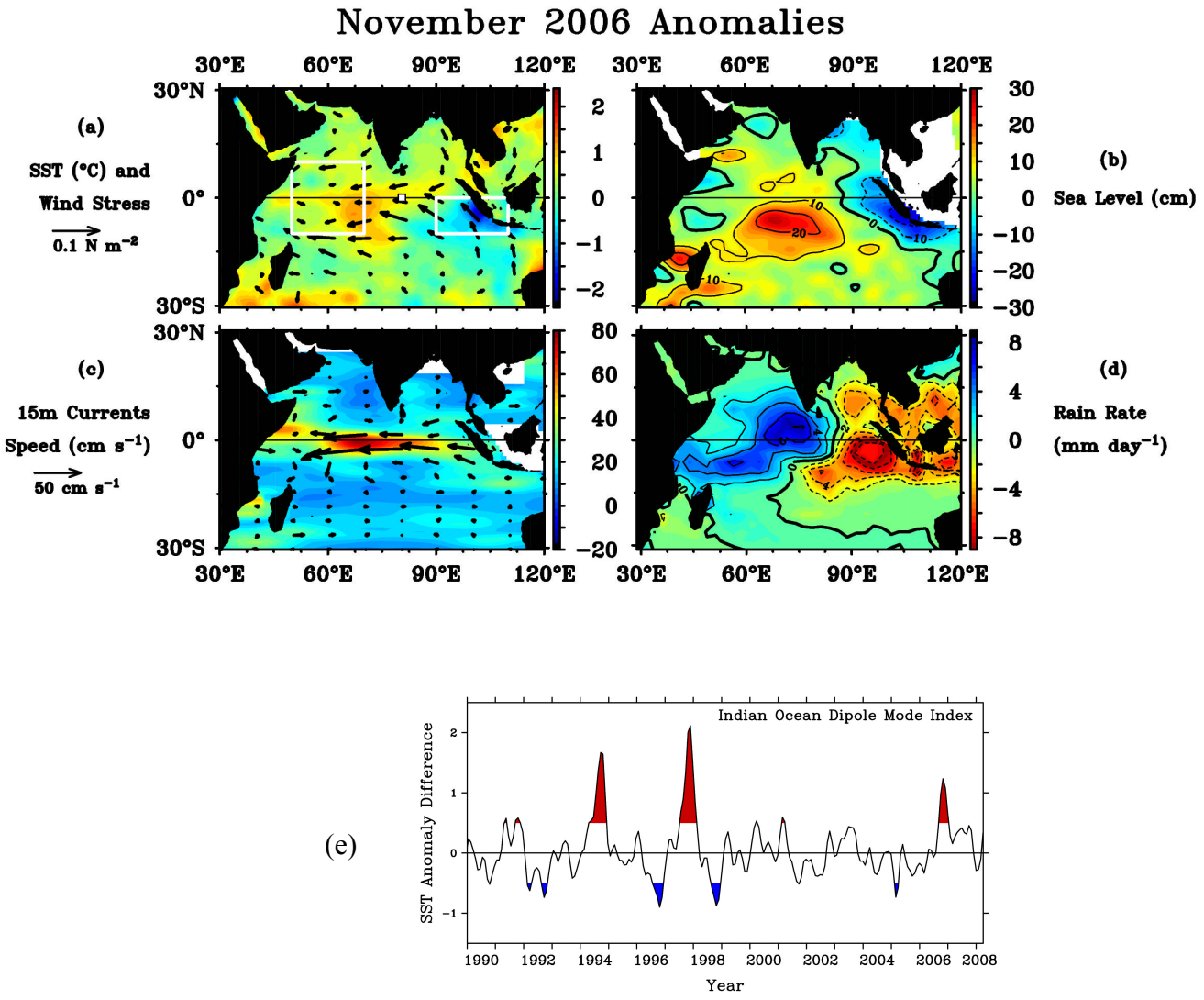

Figure 3. Monthly anomalies from the mean seasonal cycle in November 2006 for (a) SST (based on Reynolds et al., 2002) and QuikSCAT wind stress (http://www.ifremer.fr/cersat/); (b) Jason satellite altimeter sea level anomalies; (c) current velocity (vectors) and speeds (color shading) representative of flow at 15 m depth in the surface mixed layer (Bonjean and Lagerloef, 2002); (d) rain rate (Janowiak and Xie, 1999). Shown in (e) is the IODZM index for 1990-2008, with the strongest positive events (index > 0.5°C) and negative events (index is < -0.5°C) highlighted in red and blue respectively. The index represents the difference between SST anomalies in the western minus the eastern basin regions outlined in (a). Also shown in (a) is the location of an ATLAS mooring at 0°, 80.5°E, time series of which are shown in Figure 9.

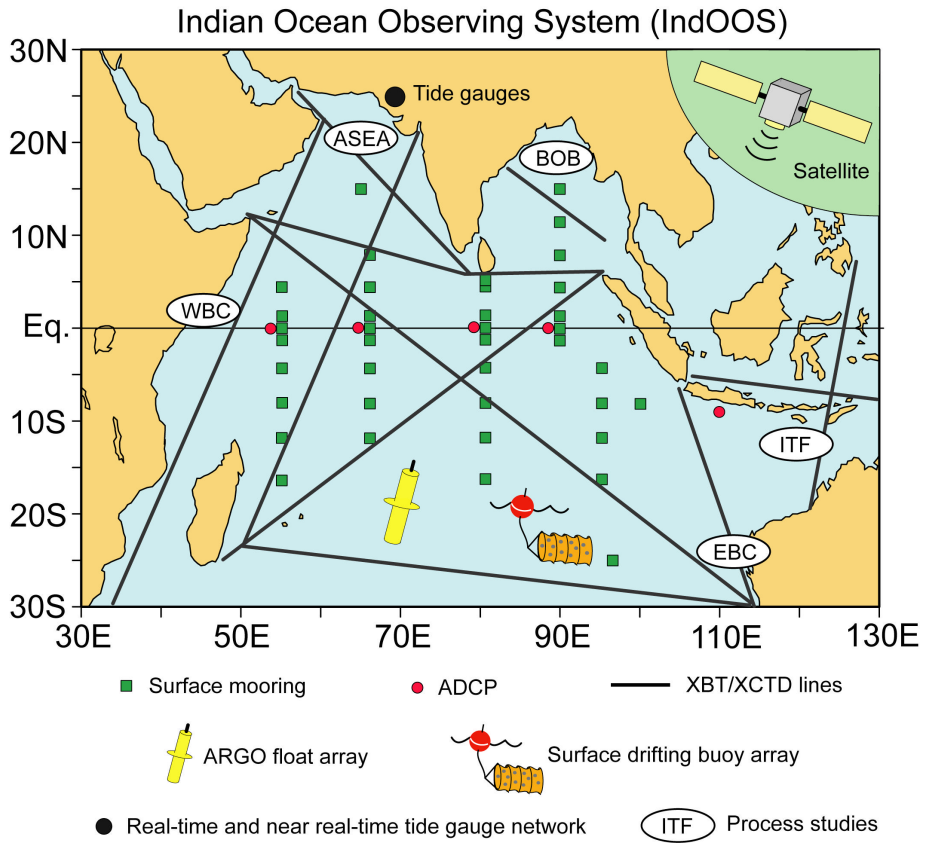

Figure 4. Schematic of the Indian Ocean Observing System (IndOOS). Expendable bathythermograph (XBT) and expendable conductivity/temperature/depth (XCTD) sections sampled by volunteer observing ships are shown as black lines. Tide gauges, Argo floats and surface drifters are indicated by a single symbol, although many of each are spread throughout the basin. Green squares indicate the locations of RAMA moorings. Process studies of limited geographical scope and duration, either completed or underway, are indicted in the ovals: Indonesian Throughflow (ITF), Western Boundary Current Studies (WBC), Eastern Boundary Current Studies (WBC), Arabian Sea (ASEA), and Bay of Bengal (BoB).

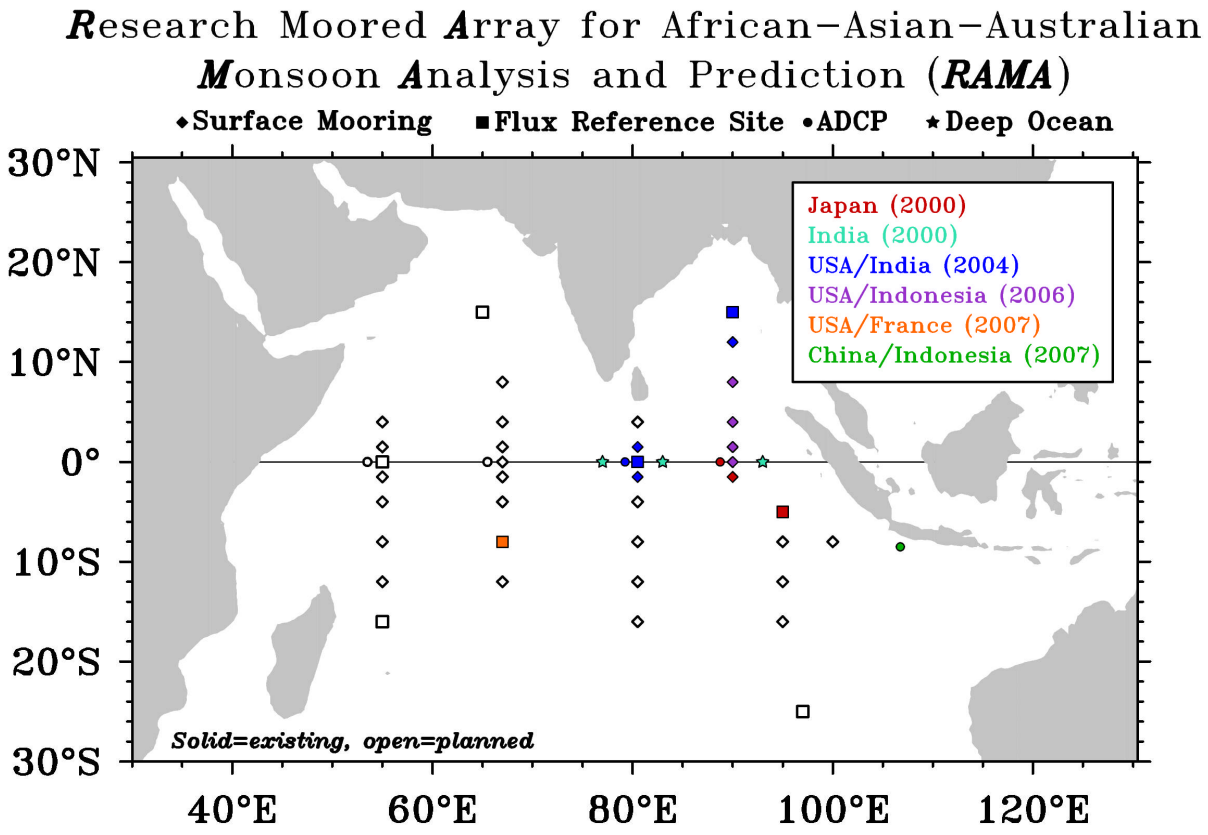

Figure 5. Schematic of RAMA. Solid symbols indicate those sites occupied so far. Color coding indicates national support, with dates of first involvement for contributing countries or bilateral partnerships shown in the upper right box. Open symbols indicate sites that are yet to be instrumented.

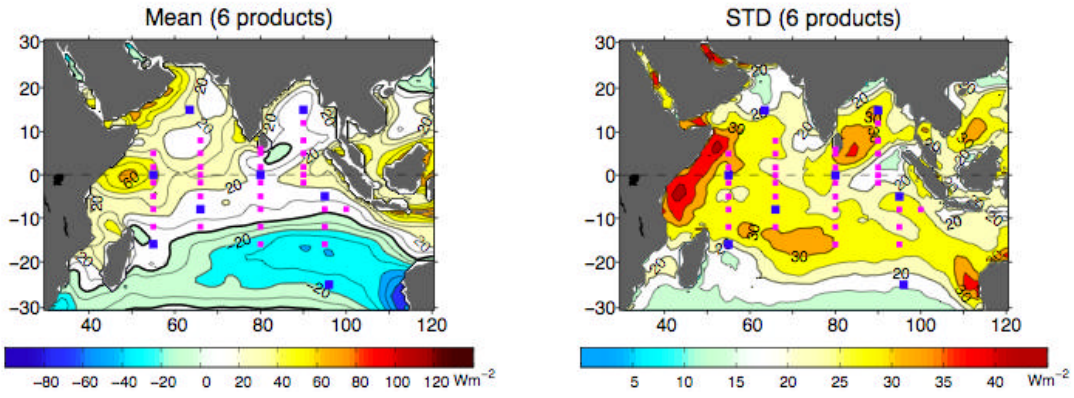

(a) (b)

Figure 6. The (a) average and (b) standard deviation of long term mean net heat fluxes from six different products. The RAMA array is superimposed on these fields with flux reference sites highlighted as blue squares. The six products are: the National Centers for Environmental Prediction NCEP1 (Kalnay et al, 1996) and NCEP2 (Kanamitsu et al, 2002) fluxes; European Center for Medium Range Forecasting (ECMWF) operational fluxes (ECMWF, 1994); ECMWF reanalysis fluxes (ERA40; Uppala et al, 2005); the U.K. National Oceanography Center (NOC) fluxes (Josey et al, 1999); and an objectively analyzed turbulent surface heat flux product produced by Woods Hole Oceanographic Institution (OA-Flux; Yu and Weller, 2007) combined with radiation data from the International Satellite Cloud Climatology Project (ISSCP; Zhang et al, 2004). Long term means for NCEP1, NCEP2, OAFlux+ISCCP, and ECMWF are based on the period 1983-2004; ERA40 means were based on the period 1983-2001 and the NOC climatology was based the period on 1980-2005.

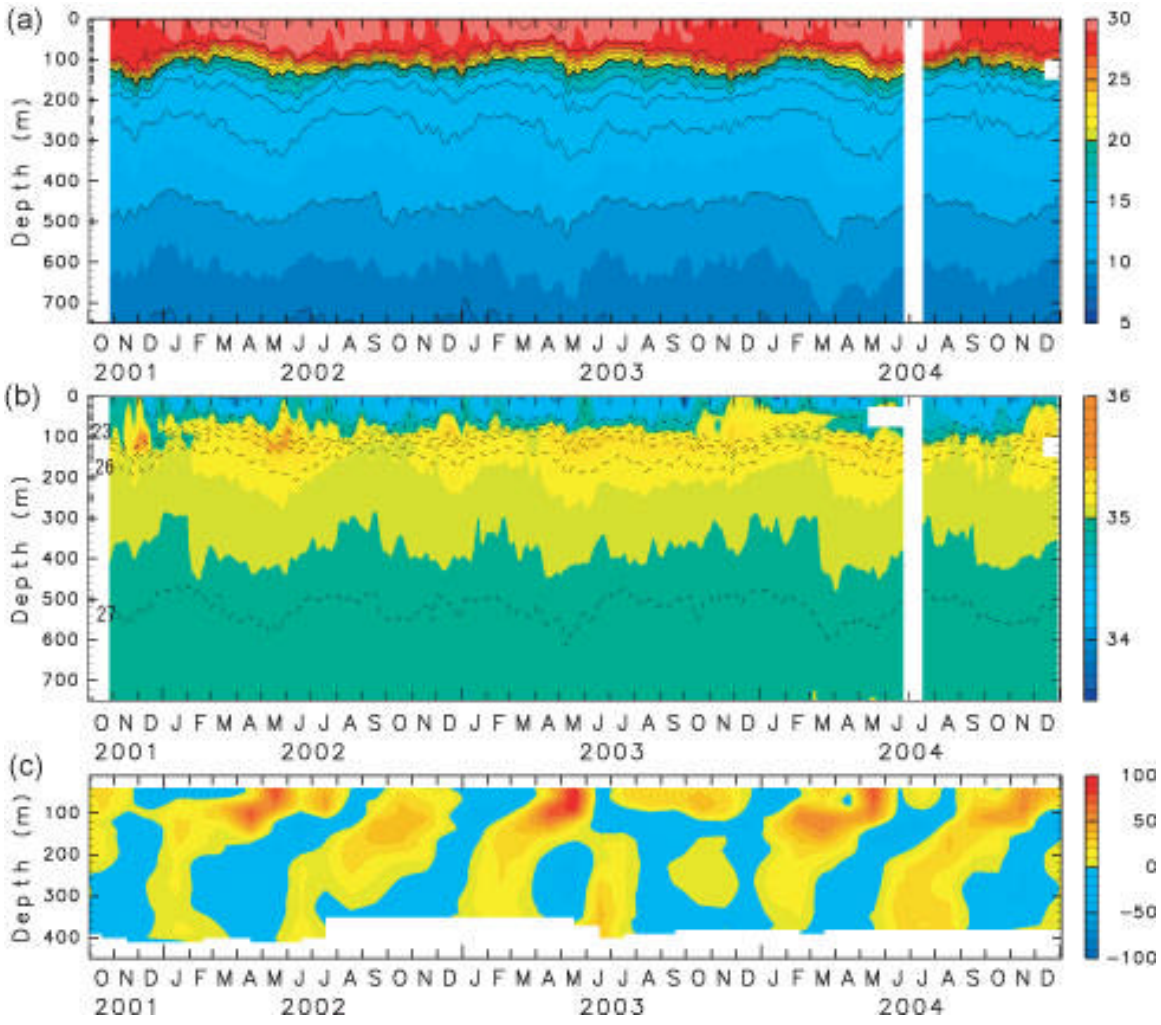

Figure 7. Time/depth sections of (a) temperature and (b) salinity from 1.5°S, 90°E and (c) zonal velocity from 0°, 90°E. Daily data in (a) and (b) have been smoothed with a 7-day running mean filter and in (c) with a monthly filter. Color intervals for the temperature, salinity and velocity are 1°C, 0.1, and 10 cm s^{-1}, respectively. Thin black lines are at intervals of 2°C for temperature with 20°C isotherm shown as a thick line. Contours of the potential density at intervals of 1.0 kg m^{-3} are superimposed on salinity sections (after Hase et al, 2008).

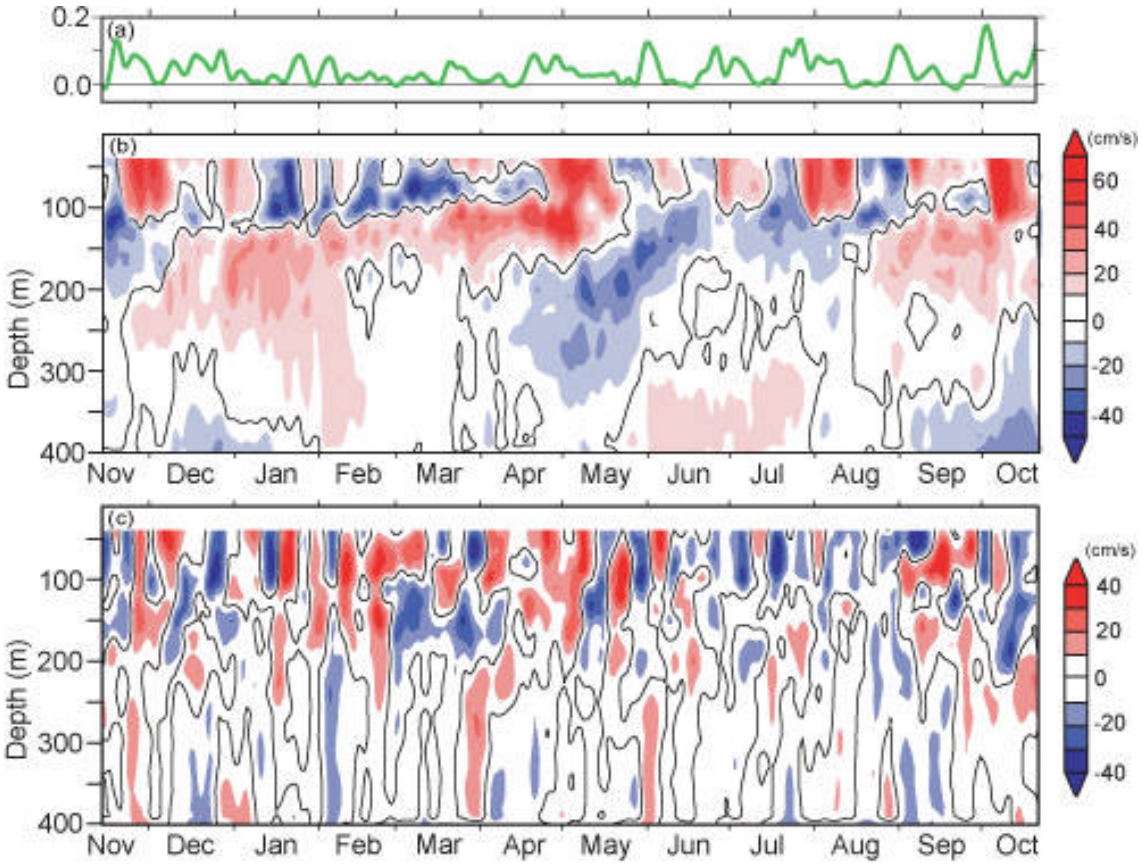

Figure 8. Time series of (a) zonal wind stress (in N m^{-2}) at the sea surface averaged between 80°E and 90°E observed by the QuickSCAT satellite. Time-depth sections of (b) zonal current and (c) the meridional current observed at 0°, 90°E. The eastward (westward) and northward (southward) currents are shaded in reds (blues), with black contours for zero velocity. Daily data have been low pass filtered with a 5-day period cut off (after Masumoto et al, 2005).

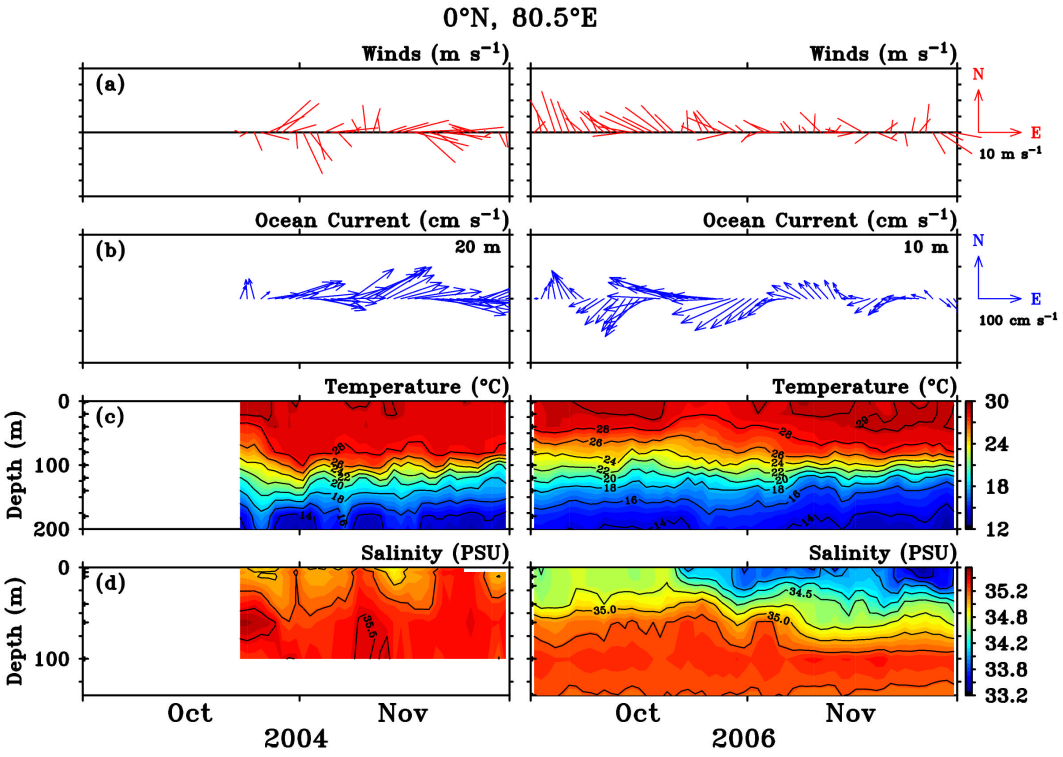

Figure 9. Daily averaged data at 0°, 80.5°E for October-November 2004 (a neutral IODZM year) and October-November 2006 (a positive IODZM year, as illustrated in Fig. 3). Shown are (a) wind vectors, (b) velocity vectors in the mixed layer (20 m depth in 2004 and 10 m depth in 2006), (c) temperature and (d) salinity. Start of the time series in mid-October 2004 is coincident with the first deployment at this site.

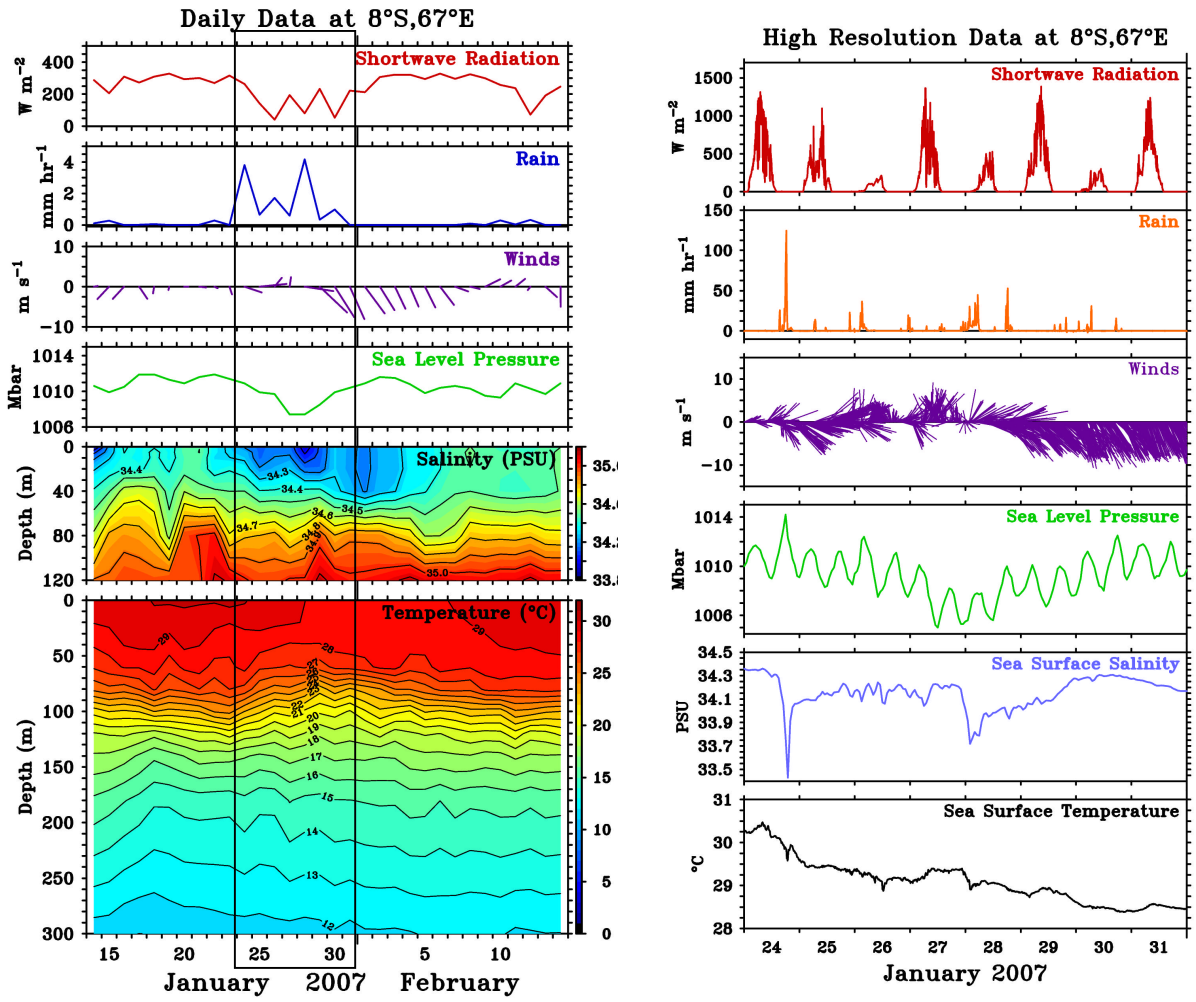

Figure 10. Time series data from 8°S, 67°E in the Seychelles-Chagos thermocline ridge region during January-February 2007. Left panel shows daily averaged real-time data whereas the right panel shows hourly averages based internally recorded data for selected variables. The period highlighted on the right coincides with the nearby passage of tropical cycle Dora in the early stages of its development.

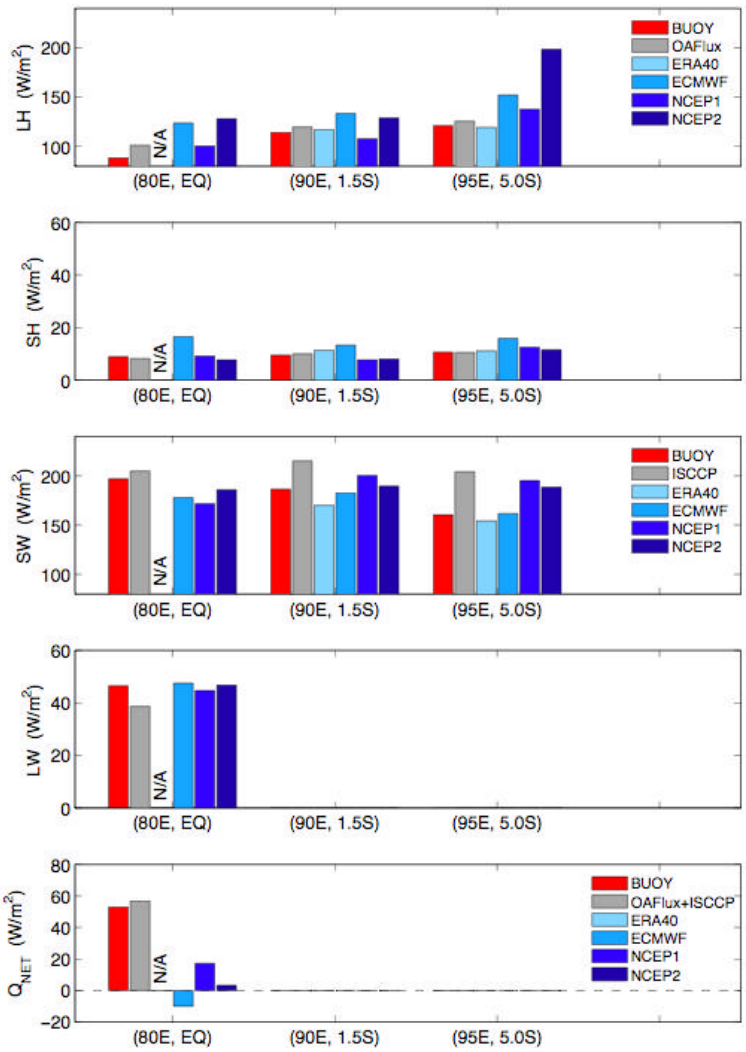

Figure 11. Comparison of surface heat flux components at three RAMA sites with those computed from six different research and operational surface flux products: NCEP1, NCEP2, ECMWF, ERA40, OA-Flux, and ISCCP (see Figure 6 caption for product definitions and references). Fluxes are, from top to bottom, latent heat flux (LH), sensible heat flux (SH), net shortwave radiation (SW), net longwave radiation (LW), and net surface heat flux (Q_{net}). Direct measurements of downwelling longwave radiation were made only at 0°, 80.5°E. Hence, LW and Q_{net} (which represents the sum of the four individual components) are shown only for this site. Turbulent fluxes were computed with the COARE version 3.0 flux algorithm (Fairall et al, 2003) using daily averaged data. No warm layer cool skin corrections were applied. Shortwave radiation was adjusted for 6% albedo. Upwelling longwave radiation at 0°, 80.5°E was computed assuming blackbody radiation from the sea surface with an emissivity of 0.97. Comparisons were based on 70 days of overlapping data at 0°, 80.5°E between 23 Oct 2004 to 31 Dec 2004; 310 days of overlapping data at 1.5°S, 90°E between 23 Oct 2001 and 31 Aug 2002; and 287 days of overlapping data at 5°S, 95°E between 26 Oct 2001 and 31 Aug 2002.